Sensitivity Analysis of Single Split Ring Resonators and Single Complementary Split Ring Resonators coupled to Planar Transmission Lines

Sensitivitätsanalyse von Einzel-Splitring Resonatoren und deren Komplementär gekoppelt an planare Leitungsstrukturen

Jesús Sánchez Pastor

Bachelorarbeit (2266-B)

General Information

Type of Thesis:	Bachelorarbeit
Thesis Title:	Sensitivity Analysis of Single Split Ring Resonators and Single Complementary Split Ring Resonators coupled to Planar Transmission Lines Sensitivitätsanalyse von Einzel-Splitring Resonatoren und deren Komplementär gekoppelt an planare Leitungsstrukturen
Thesis Number:	2266-B
Department:	Institute for Microwave Engineering and Photonics Mikrowellentechnik – Microwave Engineering
Examiner:	Prof. Dr.-Ing. Rolf Jakoby
Author:	Jesús Sánchez Pastor
Supervisor:	Carolin Reimann
Start Date:	16.05.2017
Date of Submission:	16.08.2017
Examination Date:	17.08.2017

Affidavit/Eidesstattliche Versicherung

Rechtlich bindend ist nur der deutsche Text unten. Die englische Übersetzung dient nur dem besseren Verständnis.

Hereby I assure that I made the thesis by myself without third parties' help only with the specified sources and aids. All figures, which were gathered from the sources, were marked as such. This thesis, in same or similar form, has not been available to any audit authority yet.

Hiermit versichere ich, die vorliegende Arbeit ohne Hilfe Dritter nur mit den angegebenen Quellen und Hilfsmitteln angefertigt zu haben. Alle Stellen, die aus den Quellen entnommen wurden sind als solche kenntlich gemacht worden. Diese Arbeit hat in gleicher oder ähnlicher Form noch keiner Prüfungsbehörde vorgelegen.

Place, Date

Author

Zusammenfassung/Abstract

Single Split Ring Resonators (S-SRR) and their Complementary structures (S-CSRR) are useful elements for microwave sensors for cancer detection due to their contact-less mechanism to determine dielectric properties of tissue. In this work, a basic description for both structures is provided, which involves their excitation by an electromagnetic field, their description by equivalent circuits and the influence of their design parameters on the resonance frequency. Moreover, their coupling to planar transmission lines (TL) such as microstrip lines and coplanar waveguides is described, as well as how the parameters of these transmission lines affect the excitation of the resonators. Furthermore, a figure of merit to evaluate sensitivity for resonators coupled to planar TL is defined. In order to evaluate the sensitivity for both resonator types at operating frequencies of 5 GHz, 10 GHz and 15 GHz, full wave simulations with CST Microwave Studio were performed. As a result, S-CSRR provide the highest sensitivity when coupled to microstrip lines at 5 GHz due to the larger sensing surface and high coupling to the TL. A prototype of such a structure was fabricated and 2-port measurements were done. The unloaded measured structure fitted the simulation results very well. Moreover, clear resonance shifts were detected when loading it with different materials, like Teflon, $\varepsilon_r = 2.1$, and dielectric bricks of $\varepsilon_r =$ of 15 and 20. The frequency shifts measured for them were of 1.56 GHz, 4.5 GHz and 5 GHz, respectively.

Contents

1 Introduction

Cancer is a generic term for a large group of diseases that can affect any part of the body. It is characterized by a rapid creation of abnormal cells that grow beyond their usual boundaries. It can eventually lead to the death of the patient. In 2012, cancer was directly responsible for 8.2 million deaths worldwide. Furthermore, in the same year around 14.1 million new cases were counted. In Figure 1.1, these facts are divided by countries [1]. In Europe 24.4% of worldwide new cases and 21.4% of worldwide deaths are estimated.

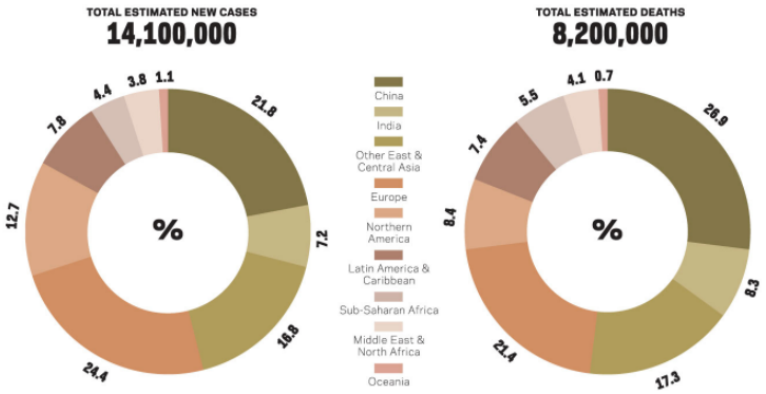

Figure 1.1: Worldwide cancer statistics in 2012

Despite the large number of new cases, between 30% - 50% of them have been prevented by avoiding risk factors such as smoking, drinking alcohol or an unhealthy diet [2]. Therefore, in order to raise the awareness of the population as well as to define standard steps to achieve an early diagnosis and appropriate treatment, several programs have been performed over the last years. The most well-known of them is the *Global Action Plan for the Prevention and Control of Noncommunicable Diseases 2013-2020*, from the World Health Organization, which aims to decrease by 25% premature mortality from cancer in 2020 [3].

In order to treat this disease, several different approaches and treatments are carried out nowadays. For instance, the detection of malignant tissue can be done with Magnetic Resonance Imaging (MRI) or Computer Tomography (CT). In addition, methods such as chemotherapy and radiotherapy are used in cancer treatment [4]. However, all of these methods might produce unhealthy side effects to the patient such as anemia, memory losses, fatigue, pain, nausea and vomiting [5]. As a way to prevent these side effects and to decrease the treatment's time and complexity, theranostic based treatments have gained more interest over the last years. These remedies consist on the combination of an individual diagnosis of the disease and personalized therapy, in order to give to the patients a specialized healthcare. This enhances the performance of the conventional methods.

One approach to achieve this theranosis treatment is the design of a microwave tool that is able to detect malignant tissue and treat it immediately after that. In this area, Split Ring Resonators (SRR), as key component of such a tool, have show promising results [6], although there are still challenges. Nevertheless, Split Ring Resonators present several advantages. Firstly, they have the accuracy of resonator-based material characterization techniques. Secondly, there is no need to apply a sample preparation process for this method to work properly. Thirdly, their dimensions are smaller compared with their resonance wavelength,

which is of great importance for the integration in a minimal invasive surgery tool. Furthermore, by using them in arrays it is possible to generate a dielectric image where each resonator corresponds to one pixel of the structure [7].

One of the key factors when designing a treatment-microwave tool using SRRs is to understand how they are excited at their resonance frequency. The resonators are coupled by an electromagnetic field to a planar transmission line. Moreover, the understanding about how the resonators distinguish between healthy and malignant tissue is important.

The aim of this bachelor thesis is to provide a general understanding about the two aforementioned topics. This work starts by offering a broad description of Single-SRRs (S-SRRs) and Single-CSRRs (S-CSRRs) in Chapter 2. In Chapter 3, the coupling of these structures to Planar Transmission Lines (TL), concretely to Microstrip Lines (MS) and Coplanar Waveguides (CPW), is explained. In addition, chapter 3 provides an explanation of how the different parameters of the TLs affect the coupling to the resonators. Chapter 4 discusses the performance of the two resonators coupled to MS and CPW in terms of sensitivity, understood as the accuracy to distinguish between different materials allocated on top of these resonators. Simulations are performed with CST MICROWAVE STUDIO and four of the simulated structures were fabricated in order to prove the results by measurements.

2 The Single Split Ring Resonator and Single Composite Split Ring Resonator

In this section, the fundamentals of S-SRR and S-CSRR are introduced. Firstly, their design parameters, resonance frequency f_0 and excitation by an ideal electromagnetic field are presented. After that, higher order resonances are addressed, as well as how the different design parameters affect the resonance frequency.

2.1 The Single Split Ring Resonator

The S-SRR consists of a conductive metallic ring, which can have different shapes like circular or square, with a non-conductive gap on it. During this bachelor thesis, Circular S-SRR are considered.

2.1.1 Definition and harmonics

When the S-SRR is placed into a temporally varying magnetic field , a circular electrical current is induced into it. This leads to an accumulation of charge across the gap of the structure, with the formation of an electric field there. This electric field opposes the induced current, causing the concentration of the magnetic field in the metallic part of the ring, with its maximum value in the opposite part of the gap [8].

A simpler way to understand the behaviour of the electric and magnetic field in the S-SRR at its resonance frequency can be depicted by its equivalent circuit, displayed in Figure 2.1 a). In resonance the reactive parts of the inductance and the capacitance compensate each other. Thus, there is a continuous circulation of the energy between these two components. This process is repeated until all the energy is dissipated due to losses of the structure.

The resonance frequency can be obtained from this equivalent circuit, as it is the frequency where the reactive parts of the capacitor and the inductor cancel out each other [9]. When this condition is applied to the circuit in 2.1 a) the resonance frequency takes the form:

$$f_0 = \frac{1}{2\pi\sqrt{L_{\text{Ring}}C_{\text{Gap}}}} \tag{2.1}$$

In order to obtain a concrete value for this frequency, the equivalent capacitance C_{Gap} and inductance L_{Ring} of the S-SRR have to be determined, by relating them to the resonator's design parameters. The resonator has four different design parameters, which are presented on Figure 2.1 b), and are:

- The radius of the inner ring, r.
- The thickness of the ring, w.
- The width of the gap, g.
- The height of the SRR, h.

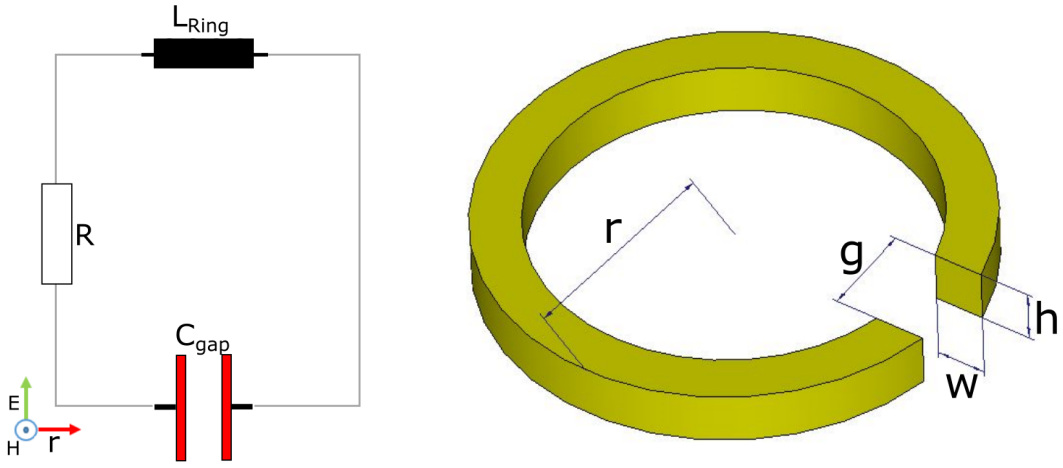

(a) Equivalent circuit (b) Sketch and parameters

Figure 2.1: SRR, equivalent circuit and parameters.

Several studies have obtained the S-SRR's resonance frequency by using a lumped circuit approximation and relating it to the design parameters, such as [10], [11], [12].

First of all, assuming the ring as a solenoid with one turn, the inductance of the ring can be calculated with:

$$L_{\text{ring}} = \frac{\mu_0 \pi R_{\text{m}}^2}{h} \tag{2.2}$$

Where μ_0 is the free-space permeability and $R_{\text{m}} = r - \frac{w}{2}$. This approximation is valid while considering a small split ($r \gg g$), which will not affect greatly the final inductance. [13]

The gap is considered as a parallel plate capacitor, thus being its capacitance:

$$C_{\text{gap}} = \varepsilon_0 \frac{hw}{g} \tag{2.3}$$

Where ε_0 is the free-space permeability. Therefore, the resonance frequency is obtained by inserting equations (2.2) and (2.3) into (2.1).

The solution of the analytical approach is compared with the resonance frequency obtained from CST Microwave Studio, in order to analyse its accurateness. The solver selected was the Frequency Domain Solver and the background distance was set to 6 mm for all directions. In Figure 2.2 a) the simulation environment with boundary definition is displayed. In order to excite the S-SRR, the boundaries of the simulation box were selected as magnetic walls (blue), $H_{\text{t}} = 0$, on the top and on the bottom of the structure, and electric walls (green), $E_{\text{t}} = 0$, on the sides of it. This way, an homogeneous electric field in the XY plane is obtained, as well as a homogeneous magnetic field in the XZ plane. Henceforth achieving the excitation by an axial magnetic field to the ring. The the design parameters used for the resonator are presented on Table 2.1.

h (mm)	**r** (mm)	**w** (mm)	**g** (mm)
0.017	5	1	0.65

Table 2.1: S-SRR, values of the design parameters

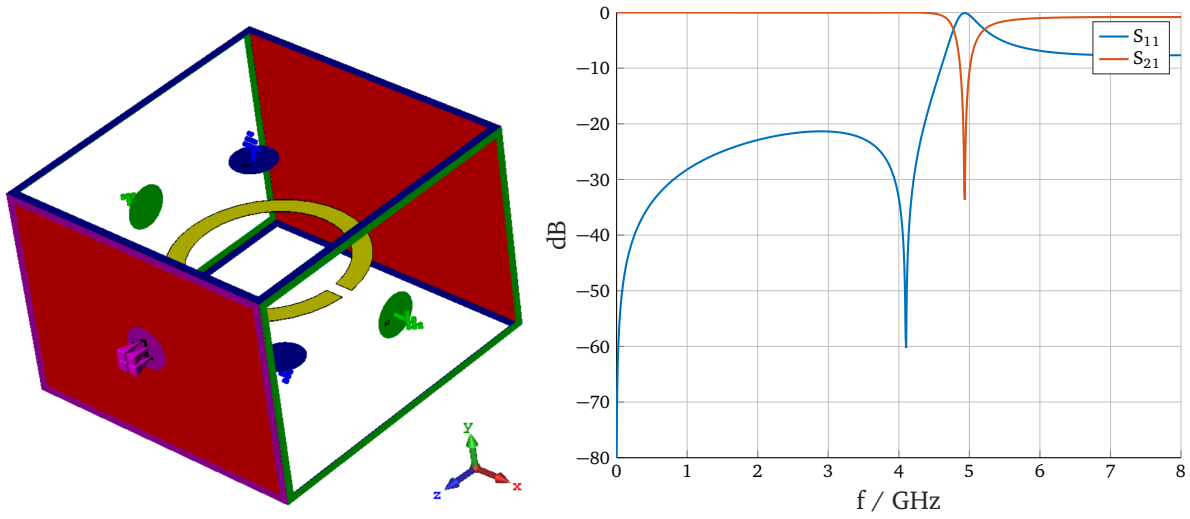

(a) Simulation environment

(b) S-parameters

Figure 2.2: SRR, simulation environment and corresponding S-parameters

The S-parameters of this structure describe the relationship between the incident voltage waves on the ports of the structure and the ones reflected and transmitted from them [9]. In other words, they give information about the amount of energy that was transmitted, or was absorbed and reflected by the structure. The reflection coefficient of the structure, S_{11}, and the transmission coefficient, S_{21} are plotted in Figure 2.2 b). They quantify the amount of energy that returns to the input port of the system and the amount that crosses it, respectively. At resonance, the energy coupled to the resonator is contained into it until it is dissipated by losses. The resonance of the designed structure is 4.9 GHz. In Figure 2.3 a comparison of calculated frequencies by using equations (2.1) - (2.3) and obtained by CST Studio for resonators with different radius between 3 mm and 10 mm is displayed.

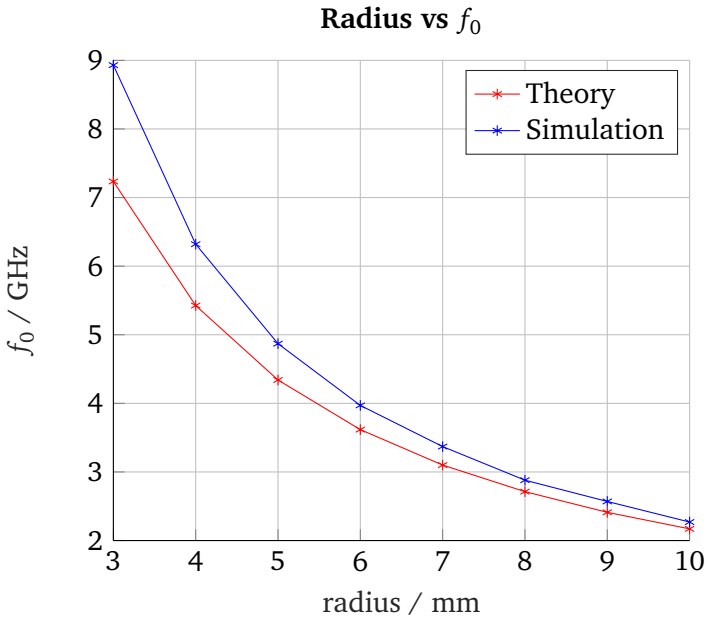

Figure 2.3: S-SRR, comparison between resonance frequencies

Especially for small radii, it can be clearly seen there is a large disagreement between both resonance frequencies. This indicates that the previously developed equations are not accurate enough. For instance, effects such as ohmic losses or fringing fields, that are not considered, affect the actual resonance frequency

value. An alternative expression able to calculate the exact resonance frequency of this kind of structures was not found in the reviewed literature. Nevertheless, the equivalent circuit presented in Figure 2.1 a) can be used to explain several effects of the resonator.

As aforestated, the resonator in Figure 2.2 a) is coupled to an homogeneous axial magnetic field and tangential electric field. Since the gap-axis of the resonator is oriented in the same direction of the incident electric field, its contribution to the structure will be minimum although not zero. This is due to the reflections of the incident field on the S-SRR, as it is a good conductor, that cause the coupling of the field to the vicinities of the gap. Furthermore, when the structure is rotated the influence of the incident electric field grows. This modifies slightly the previously existent field in the gap. Thus the current distribution is also lightly modified.

As a consequence of this phenomenon, a small shift in the resonance frequency is provoked. In Table 2.2 the resonance frequency for different values of θ are displayed, where θ is the rotation angle of the S-SRR. Figure 2.4 shows the derived equivalent circuits for the corresponding resonators for $\theta_1 = 0°$, $\theta_2 = 45°$ and $\theta_3 = 90°$, respectively. From Table 2.2 can be extracted thath the resonance behaviour is symmetric.

θ	0°	45°	90°	135°	180°	225°	270°	315°
f_0 (GHz)	4.90	4.96	5	4.96	4.90	4.96	5	4.96

Table 2.2: S-SRR, changes of resonance frequency with angle

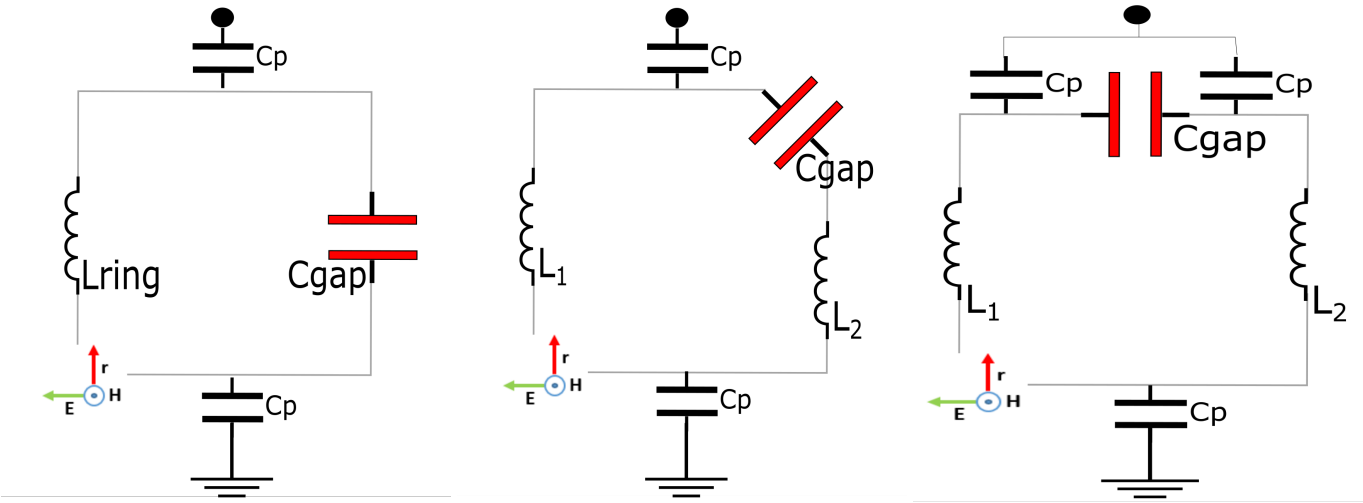

(a) Equivalent circuit for $\theta = 0°$ (b) Equivalent circuit for $\theta = 45°$ (c) Equivalent circuit for $\theta = 90°$

Figure 2.4: S-SRR, equivalent circuit for different angles

In Figure 2.4, C_p accounts for the parasitic capacitance between the resonator and the side-boundaries of the simulation box. By rotating the resonator, the total inductance L_{ring} is distributed along the metallization, which is reflected in the equivalent circuit. If the parasitic capacitances are considered to be zero, $C_p \to 0$, these different inductances will add up, $L_{ring} = \sum_{i=1}^{N} L_i$, resulting in the same value for the three circuits. This might lead to the conclusion that the small differences between the resonance frequencies for each angle in Table 2.2 are due to these parasitic capacitances. The boundaries in the simulation box were set sufficiently far to achieve the condition $C_p \to 0$. Thus coming these differences from the coupling between the tangential electric field and the resonator [14].

In Figure 2.5, the first and second order harmonics for the aforementioned θs are displayed. From this graph, there are two noticeable differences between the S-parameters for the rotations of the resonator.

First of all, there is a peak that vanishes in the reflection coefficient for f = 4.09 GHz and rotations different of 0°. This is caused by a phase shift of the reflected waves along the resonator. From the equivalent circuits

presented in Figure 2.4 a) and c), it is seen that for $\theta = 0°$ the equivalent circuit has no symmetry respect the propagation direction of the signal, indicated with the red arrow r. This means that the capacitor and the inductor are introducing a different phase shift to the reflected signals along the circuit, which is making them interfere destructively. On the other hand, in the equivalent circuit for $\theta = 90°$, Figure 2.4 c), the resonator is symmetric regarding the propagation direction. Thus the phase shift introduced in the reflected signals has the same value, hence they do not cancel each other.

The other relevant difference between the S-parameters is the suppression of the second resonance for $\theta = 90°$. In this harmonic at this angle, the surface currents on the resonator have the same direction and phase, and the electric field of the gap is not able to counteract them. Consequently, the reactive parts of the capacitance and inductance do not cancel out each other. This is presented in Figure 2.6 a). However, for the third resonance the wavelength fits three times in the structure. This changes the direction of the surface currents in such a way that they compensate each other, achieving the resonance at that frequency. As a consequence, when $\theta = 90°$, all the resonances corresponding to the even multiples of the wavelength are suppressed. Figure 2.6 b) shows the surface currents for this harmonic, located at 15.4 GHz. It is noticeable that for a) the surface current follows the same direction along the ring, whereas for b) the current on the bottom part opposes the other two.

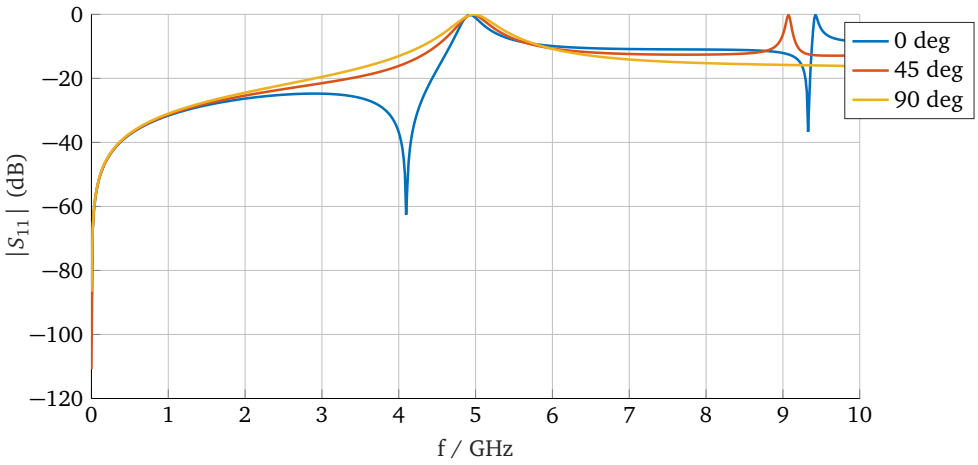

(a)

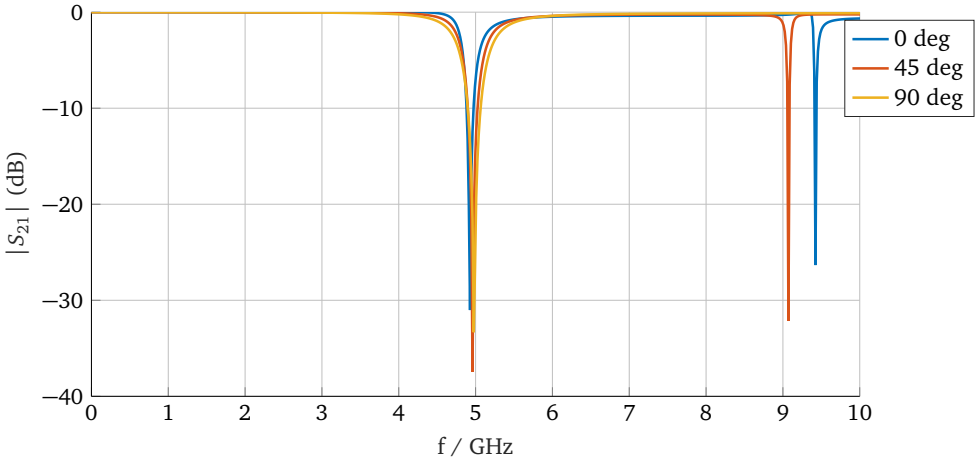

(b)

Figure 2.5: S-SRR, harmonics for rotations of the ring

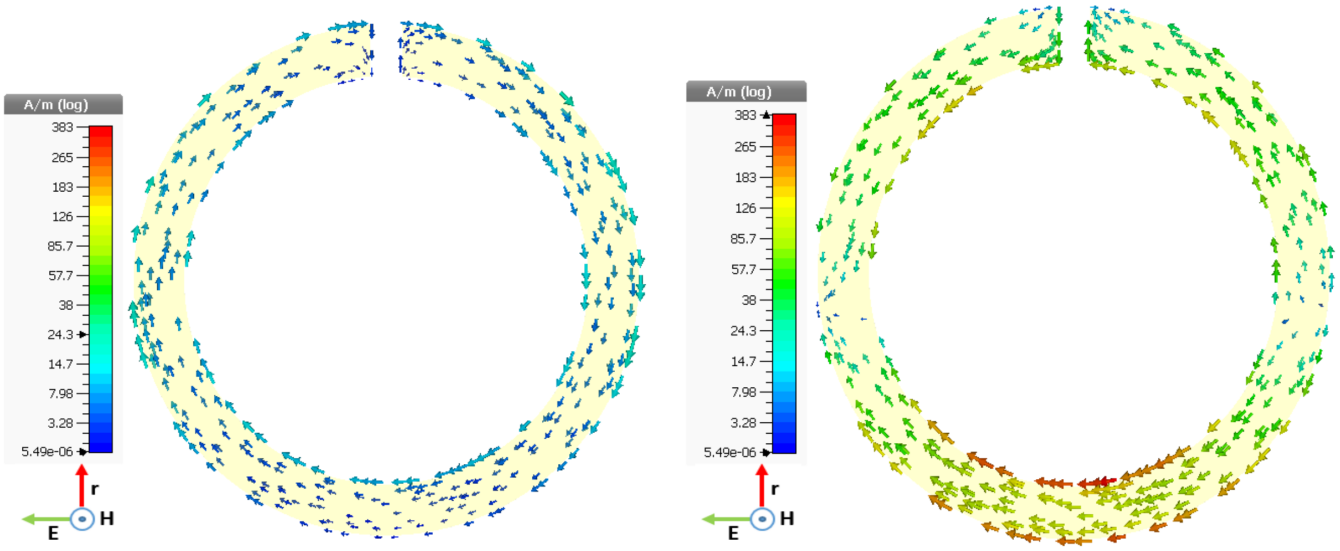

(a) Supressed second harmonic, $f = 9.5$ GHz

(b) Third harmonic, $f = 15.4$ GHz

Figure 2.6: S-SRR, surface current distribution for $\theta = 90°$

2.1.2 Influence of design parameters

When the design parameters of a S-SRR are modified a shift in its resonance frequency is produced. This is caused by the modification of the inductance and capacitance of the structure. For instance, if the width of the split is increased, the self-capacitance of the structure is smaller, leading to an increase of the resonance frequency. In this section, infuences of design parameters are addressed. The metallization height is fixed to h = 0.017 mm due to fabrication constrains, and the angle θ is set to 0°.

Changes with the radius

S-SRRs are able to support resonance wavelengths λ_0 whose dimensions are larger than the length of the resonator. For instance, the resonance wavelength of the previously described S-SRR, with has a diameter of 9 mm, is:

$$\lambda_0 = \frac{c}{f_0} = 61.25 \text{ mm} \tag{2.4}$$

Where c is the speed of light in vacuum. Despite this, the radius of the ring is a critical parameter to design the resonance frequency of the structure, as it will make its length smaller or larger, consequently changing the resonance wavelength. Figure 2.7 a) presents this effect for eight different simulations of r between 3 mm and 10 mm. As expected, the larger the radius, the smaller the resonance frequency is.

Changes with width of the gap

As it is explained before, the gap can be considered as a capacitor. Thus, the larger the gap width is, the smaller the corresponding capacitance is. In addition, the inductance is also lower, as the amount of metallization decreases. This shifts the resonance frequency towards higher values [15]. In Figure 2.7 b) the results are plotted for five different gap distances between 0.25 mm and 1.05 mm. The simulated results follow the previous statement.

Changes with width of the resonator

The inductance of the system is inversely proportional to the width of the ring. For large ring widths its value is decreased. Although the capacitance increases consequently, the influence of the inductance in the resonance frequency is more relevant. Thus, the resonance frequency is shifted towards higher values the thicker the resonator is. This behaviour has been studied for five equidistant resonator widths between 0.5 mm and 1.5 mm and plotted on Figure 2.7 c). It is seen that the resonance frequency is shifted towards higher frequencies the wider the resonator.

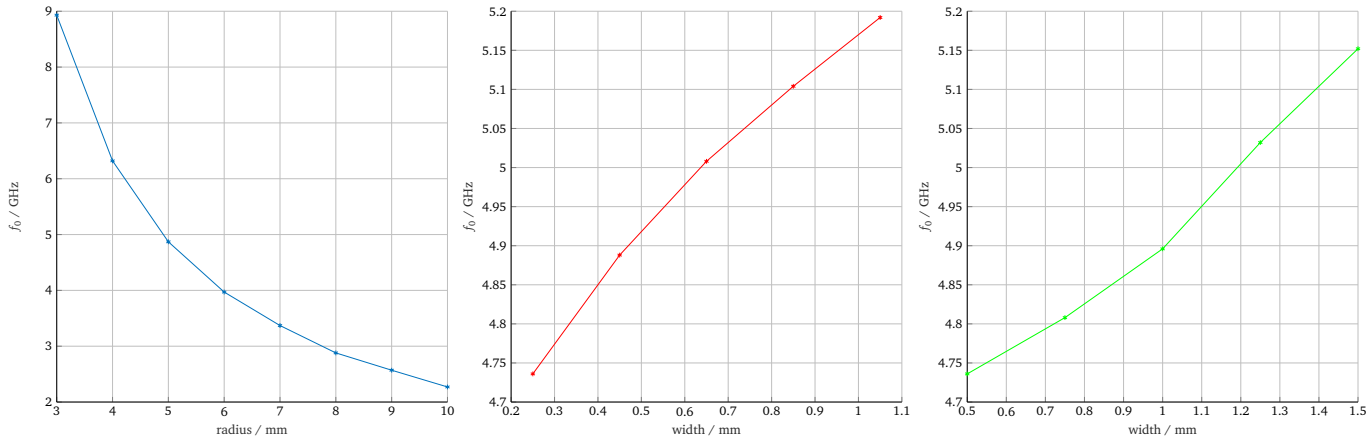

(a) Radius vs f_0 (b) Gap width vs f_0 (c) Ring width vs f_0

Figure 2.7: S-SRR, influence of the design parameters on f_0

Changes with the substrate height and permittivity

When the resonator is loaded with a substrate, its resonance frequency is shifted towards lower values. This shift depends on the relative dielectric permittivity ε_r of the substrate material. A material with a high ε_r is able to constrain more electric field inside it that one with lower ε_r, thus increasing the shift towards lower frequencies further than the former one.

Moreover, the substrate height also affects this shift. As its value grows, more field of the SRR is contained in the substrate, until all the field in the half space where the substrate is present is pulled into it. For this height, and for the ones that are larger than it, the resonance frequency does not change, since the effective permittivity of the resonator remains constant. Figure 2.8 exposes this behaviour for two different substrates, Rogers RT6010, $\varepsilon_r = 10.2$, and Rogers RO4003C, $\varepsilon_r = 3.38$. As it is expected, the resonance frequencies for the resonator on RO4003C are allocated in higher values than the one loaded with RT6010. There also is a value for the substrate height where the resonance frequency does not change anymore. Its final value for each substrate is $f_{\text{RO4003C}} = 3.39$ GHz and $f_{\text{RT6010}} = 2.1$ GHz. In contrast, the frequency for the unloaded S-SRR is $f_{\text{unload.}} = 4.9$ GHz. The shift that is experimented is more than 1 GHz for both cases. Since it is normally necessary to put the S-SRR in the top of a substrate for fabrication or measurements, the omission of it when simulating leads to relevant discordances between the simulated and real results.

2.2 The Single Complementary Split Ring Resonator

The Complementary SRR is the reverse image of the SRR. Therefore, the ring is formed by a non-conducting material, surrounded by a conductive plane. Its behaviour can be explained by the Babinet Principle.

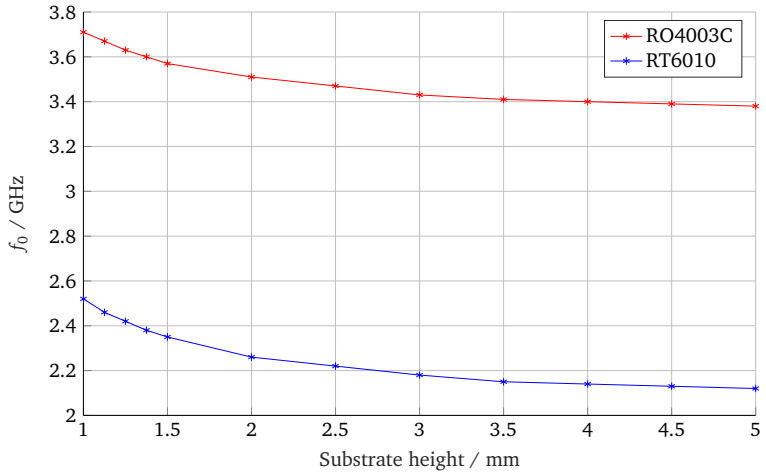

Figure 2.8: S-SRR, influence of the substrate height on f_0

The Babinet principle states that the diffraction pattern from an opaque body is identical to that from a hole of the same size and shape except for the overall forward beam intensity [16]. Extended to the electromagnetic field, there is an inversion of the fields between a structure and its complementary. The magnetic field distribution substitutes the previous electric field and vice versa [17] [18]. Nevertheless, the resonance frequency remains unchanged for lossless conductors.

2.2.1 Definition and harmonics

Following the Babinet principle, the excitation of a S-CSRR is achieved by coupling it to a axial electric field. This field creates differences of potential along the whole surface, which results in induced currents between these voltage gradients. The surface currents generate a electric field between the sides of the ring, as it is a non-conductive material. Although the capacitance of the S-CSRR is larger than the S-SRR, there is no shift of the resonance frequency as the inductance of the structure decreases accordingly. The magnetic field coils around the gap, which is now metallic.

At resonance, the behaviour is exactly the same as the S-SRR, with the energy twirling from the inductor to the capacitor and vice versa. In Figure 2.9 a) is displayed the equivalent circuit of this resonator. The capacitance is the one inherent to the dielectric ring, whereas the inductance comes from the metallic plane. Figure 2.9 b) shows the S-parameters for the Complementary of the first resonator presented in section 2.1.1, whose design parameters are on Table 2.1.

The resonance frequency for this structure is slightly different from its SRR counterpart, 4.96 GHz versus 4.90 GHz, respectively. This is caused due to the larger presence of copper, that affects the loses of the system. In the simulation, a symmetry magnetic plane was defined, in order to excite a plane wave with desired electric and magnetic field components. The reason for this is that the conductor sheet is fixed at the same place than the ports, in order to prevent reflections that distort the S-parameters of the structure. However, this provoked a shortcut in the ports, with the appearance of degenerated input modes, instead of the TE_{01}. In Figure 2.9 c) the CST set up is displayed. The size of the metallic part outside the ring is set to 6 mm.

When the ring is rotated, the input magnetic field coupling to it grows stronger. This changes slightly the resonance frequency of the resonator. In Table 2.3 the values for the resonance frequencies in dependency of the angle are shown.

In opposition with Table 2.2, there is no symmetry with respect to the different angles. This is caused by the losses on the metal part, which are higher than in the previous cases, as well as a slightly differences in the surface current distribution for each case. Nevertheless, the shift between complementary angles is not

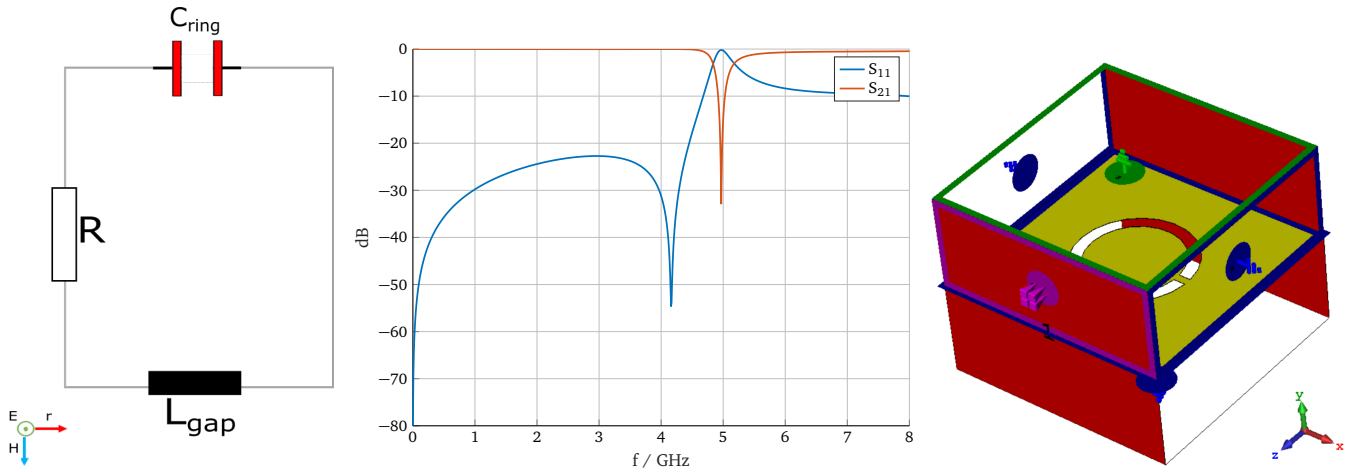

(a) Equivalent circuit (b) S-parameters (c) Simulation environment

Figure 2.9: S-CSRR, equivalent circuit, corresponding S-parameters and CST set-up

θ	0°	45°	90°	135°	180°	225°	270°	315°
f_0 (GHz)	4.912	5.024	5.208	5.04	4.92	5.056	5.176	5.048

Table 2.3: S-CSRR, changes of resonance frequency with angle

relevant. Therefore, higher order harmonics are studied for the same rotations of Section 2.1.1. Figure 2.10 shows the S-parameters for $\theta = 0°$, 45° and 90°. From this Figure, it is possible to see the same effects that are explained for the S-SRR in the previous section.

Firstly, there is a minimum peak in the reflection coefficient for $\theta = 0°$. The reason of this behaviour is the same for the S-SRR. The phase of the reflected waves is shifted, which makes them to interfere destructively when returning to the input port. This effect disappears when the path that they follow is symmetric respect the direction of propagation, which happens for $\theta = 90°$.

Secondly, for $\theta = 90°$ there is no second harmonic. Similar to the S-SRR, the reactive parts of the inductance and capacitance are not compensating each other. Thus, the second harmonic is not being excited. In Figure 2.11 the electric field distribution on the non-conductive gap is shown. The section a) corresponds to the suppressed second harmonic at $f = 10.5$ GHz, whereas the b) is the electric field for the third harmonic at 16.44 GHz. As expected, the resonance wavelength fits three times correspondingly.

2.2.2 Influence of design parameters

As explained in 2.1.2, there is always a change in the resonance frequency when modifying the design parameters of the resonator. However, it is important to know whether this shift is the same for the S-SRR and the C-SRR when modifying the same parameters. If the Babinet principle is considered, this affirmation should be correct.

Changes with the radius

S-CSRRs are, like their counterparts, able to support resonance wavelengths whose dimensions are larger than the structure. If their radius is decreased, the structure is made shorter. Thus the length of the resonance wavelength that can propagate into it decreases. This makes the resonance frequency to shift towards higher values. Figure 2.12 a) displays this behaviour for different values of the radius between 3 mm and 8 mm. It is easily seen that the resonance frequency decreases inversely with the radius.

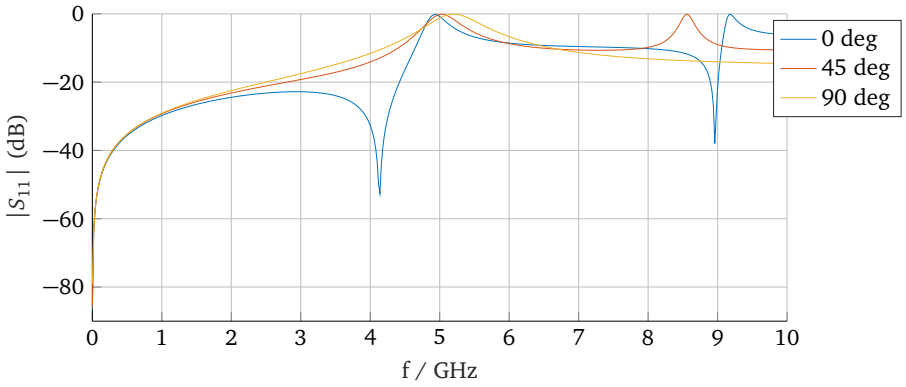

(a)

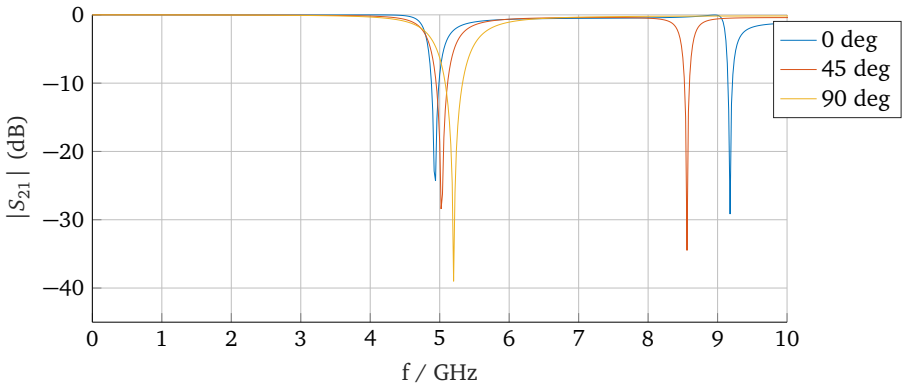

(b)

Figure 2.10: S-CSRR, harmonics for rotations of the ring

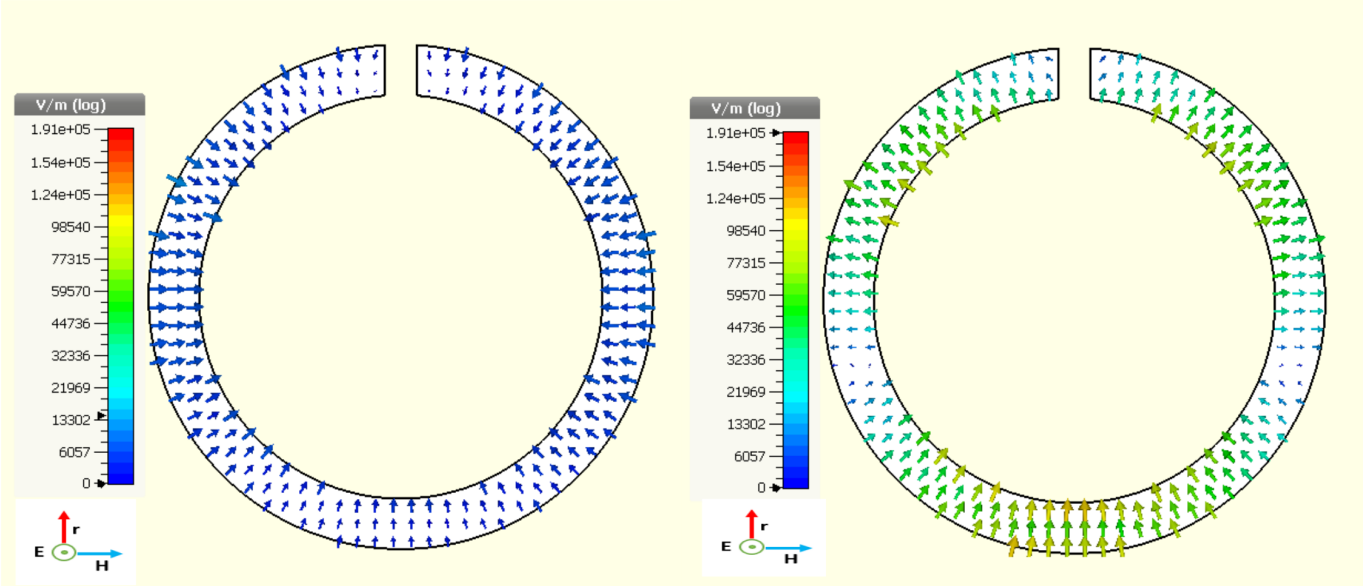

(a) Supressed second harmonic, $f = 10.5$ GHz

(b) Third harmonic, $f = 16.44$ GHz

Figure 2.11: S-CSRR, electric field for $\theta = 90°$

Changes with width of the gap

Modifying the width of the gap has a direct influence in the inductance and capacitance of the system. For instance, the smaller the width, the higher the inductance inherent to the metallic gap. The capacitance of the structure is increased as well, as the surface of the dielectric ring grows. Therefore, for larger values of gap width, higher resonance frequencies are expected. Figure 2.12 b) confirms this assessment for gap widths between 0.25 mm and 1.05 mm.

Changes with width of the resonator

As it is explained before, the ring of the resonator is made by a dielectric material. Consequently, by varying this parameter the capacitance is changed. When the width of the ring is decreased, the capacitance grows, and vice versa. Although the inductance of the system grows the thicker ring is, the change is too small to be able to compensate the decrease of the capacitance. For this reason, the resonance frequency increases the wider the ring is. In Figure 2.12 c) this change is addressed and confirmed for values between 0.5 mm and 1.5 mm.

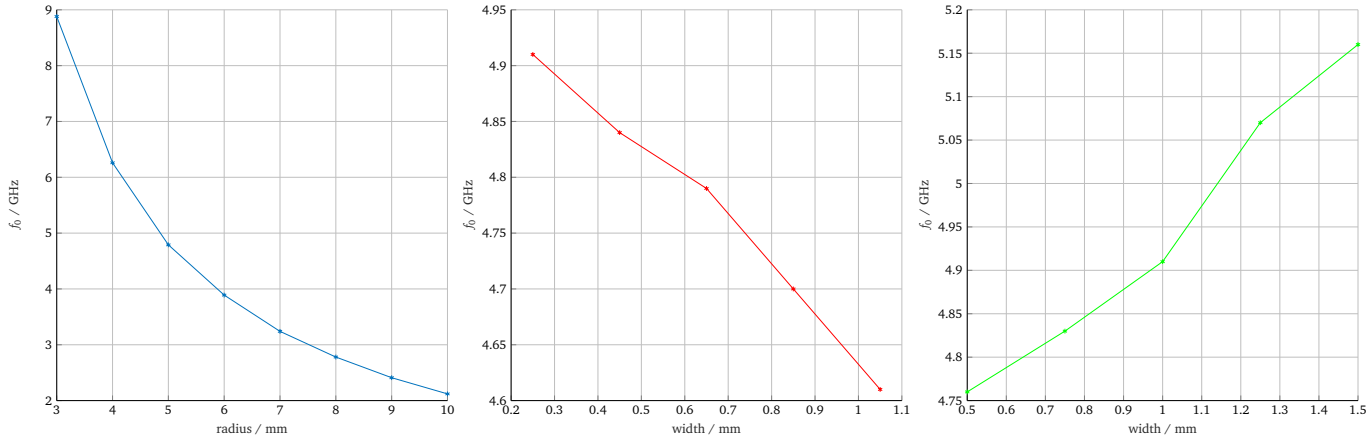

(a) Radius vs f_0 (b) Gap Width vs f_0 (c) Ring Width vs f_0

Figure 2.12: S-CSRR, influence of the design parameters on f_0

Changes with the substrate height

As explained in section 2.1.2, when the resonator is loaded with a substrate, its resonance frequency is shifted towards lower values, depending of the ε_r of the material and the height of the substrate. Therefore, the same results as the obtained for the S-SRR are expected. Figure 2.13 exposes this behaviour for two different substrates, Rogers RT6010, $\varepsilon_r = 10.2$, and Rogers RO4003C, $\varepsilon_r = 3.38$. It is seen that the previous statement is confirmed.

2.3 Summary of both resonators

This section aims to briefly summarize and compare the previously explained resonators, whose most important characteristics are displayed on Table 2.4.

As a quickly reminder and in order to clarify the table, θ is the angle of the rotation that the resonator experiments respect the incident electric field, in the case of the S-SRR and the incident magnetic field,

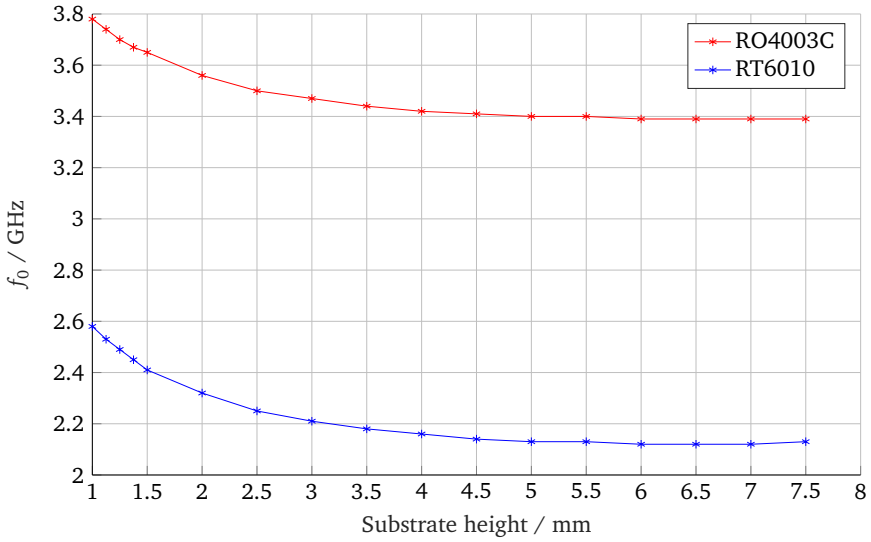

Figure 2.13: SCSRR, influence of the substrate height on f_0

for the S-CSRR. Morevoer, in the equivalent circuits the yellow color is meant to represent metallization, whereas the white one dielectric. Finally, the influence of the design parameters in the resonance frequency are not considered, as they have the same effect in both resonators.

	S-SRR	**S-CSRR**
Ring	Metallic	Complementary
Main excitation cause	Axial magnetic field to the ring	Axial electric field to the ring
Resonance frequency	$f_0 = \frac{1}{2\pi\sqrt{L_{\text{ring}}C_{gap}}}$	$f_0 = \frac{1}{2\pi\sqrt{L_{gap}C_{ring}}}$
Second order harmonic	For $\theta = 90°$, second harmonic suppression.	Same behaviour.
Equivalent Circuit	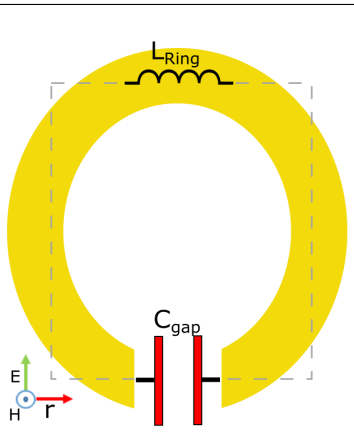	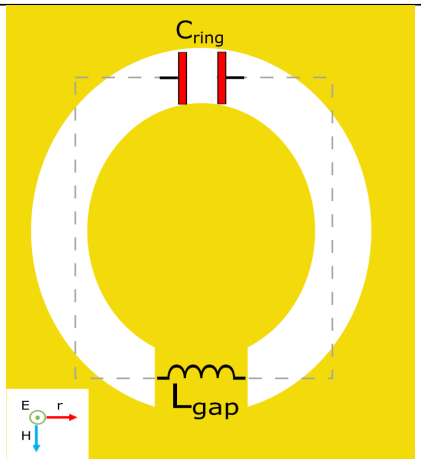

Table 2.4: Comparison between both resonators

3 Coupling to Planar Transmission Lines

In order to detect and treat cancer with a minimal invasive microwave applicator, the devide is inserted into the targeted malignant tissue. The resonators have to be excited inside the patient body and their reflection parameters have to be measured once into it. The straightforward solution to this matter is to couple the resonators to a planar transmission line, such as a microstrip line or a coplanar waveguide. The transmission line is connected to a coaxial cable which is directed to an external source outside the body, whereas the resonator is in the part of the line that is inside the tissue. By using the electromagnetic field inherent to these two transmission lines and properly allocating the resonator on them, their excitation is achieved.

This chapter addresses the coupling of S-SRRs and S-CSRRs to microstrip lines and coplanar waveguides. First of all, a criteria to measure the coupling strength is explained. After that, the characteristics of the lines are briefly described. Finally, the coupling of S-SRR and S-CSRR is addressed at resonance frequencies of 5 GHz, 10 GHz and 15 GHz.

All the simulations in this chapter are 2-Port simulations where the Time Domain Solver in combination with the AR filter is used. Moreover, the background distance is set to 7.5 mm and the boundaries to open. The target is to evaluate the S-parameters of the structures when only one parameter of the TL is changed, whereas the rest remain constant.

3.1 Coupling Evaluation

For the study of the coupling for both planar transmission lines, it is necessary to develop a parameter that is able to measure the strength of the coupling between the transmission lines and the resonators.

When a resonator coupled to a transmission line is excited, a minimum peak in $|S_{21}|$ at the resonance appears. As it is explained in Section 2.1.1, there is a part of the input signal that does not cross the structure, but is coupled to the S-SRR or the S-CSRR until it is dissipated by losses. The value of the peak on $|S_{21}|$ depends in the signal energy that is contained in the resonator. As this S-parameter quantifies the amount of energy that has passed over the TL, the value of its peak at resonance is smaller for strong coupling between TL and resonator.

In lights of the above, the minimum peak value of $|S_{21}|$ at the resonance frequency is a good option to study the coupling between a resonator and a transmission line. However, it is important not to confuse it with the coupling coefficient between two resonance structures, which is given by

$$k = \frac{|f_2^2 - f_1^2|}{f_2^2 + f_1^2} \tag{3.1}$$

This factor accounts for the coupling between two resonance frequencies, whereas the $|S_{21}|$ peak at resonance stands for the quantity of input signal energy stored in the resonator.

3.2 The Microstrip Line

The first microstrip line was presented in the IRE proceedings of 1952 by Grieg and Engelmann. Since then, it has become one of the most used planar transmission lines for microwave and radiofrequency circuits. Microstrips are well-known for their planar nature, which allows an easy fabrication for different structures, combined with good heat sinking and mechanical support, as well as uncomplicated integration with solid stated devices. Due to these reasons, a lot of investigations and work in these structures has been carried out since they appeared, such as [9, 19, 20, 21].

3.2.1 Definition

Microstrip transmission lines are formed by a conductive strip of width w and thickness t and a ground plane. This plane is usually wider than the strip and it is separated by it with a dielectric layer with height h. Figure 3.1 displays the basic layout of this transmission line.

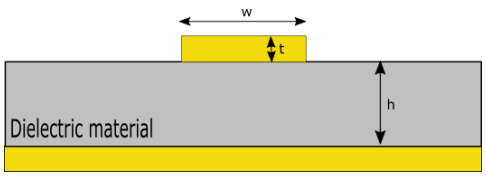

Figure 3.1: Microstrip line layout

As it was stated before, the microstrip line has several positive aspects which make it especially useful for microwave engineers. However, they also show several special characteristics due to their nature that should be taken into account.

Firstly, they are the rectangular version of a wire over a ground plane. In other words, they radiate energy, which can give place to unintended circuit responses. An experimental rule to minimize this behaviour is to decrease the substrate height to at least one tenth of the operating wavelength, h $< \lambda_{op}/10$.

Secondly, the electromagnetic field of the microstrip is characterised by the apparition of fringing fields. There is a part of the EM field density that does not stay between the ground and the strip, but propagates outside it. As a consequence, a pure TEM cannot propagate in this transmission line. In Figure 3.2 its EM is displayed. It is easily noticeable the presence of field components outside the structure.

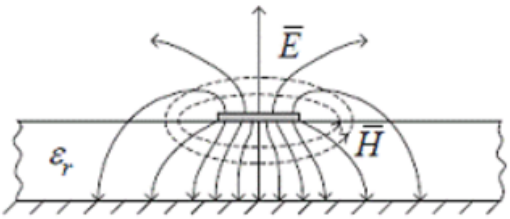

Figure 3.2: Microstrip line, sketch of EM field from [22]

As a consequence of not being able to support a pure TEM mode, the line becomes dispersive. Thus, the phase velocity, characteristic impedance and field across the line are not constant, but they show a dependence on frequency. This behaviour becomes more noticeable the smaller the ratio w/h is.

Finally, in order to be able to calculate which wavelengths are propagating inside the structure, a new concept is required to be developed to account for the fringing fields of the microstrip. Therefore, the effective

dielectric constant, ε_{eff} is used. It is directly dependent of the substrate relative dielectric permittivity and the ratio h/w.

$$\varepsilon_{\text{eff}} = \frac{\varepsilon_{\text{r}}+1}{2} + \frac{\varepsilon_{\text{r}}-1}{2}\frac{1}{\sqrt{1+12\frac{h}{w}}}, \quad \text{when} \quad \frac{w}{h} > 1 \quad \text{and} \tag{3.2}$$

$$\varepsilon_{\text{eff}} = \frac{\varepsilon_{\text{r}}+1}{2} + \frac{\varepsilon_{\text{r}}-1}{2}\left[\frac{1}{\sqrt{1+12\frac{h}{w}}} + 0.04\left(1-\frac{w}{h}\right)^2\right], \quad \text{when} \quad \frac{w}{h} < 1 \tag{3.3}$$

These equations ignore the strip thickness. However, it is normally a good approximation to calculate ε_{eff}. From this expression it can be implied that the value of the effective dielectric constant is always between $\frac{\varepsilon_{\text{r}}+1}{2}$, when $h/w \to \infty$, and the one of the substrate, when $w/h \to 0$.

When the central strip is wide enough in relation to the substrate height, the dispersion is minimum and the microstrip line behaves as a parallel plate capacitor. For this case, $\varepsilon_{\text{eff}} \approx \varepsilon_{\text{r}}$. This means that most of the electromagnetic field of the line is contained between the strip and the ground. In contrast, the thinner the strip is, the more fringing fields are outside the structure, and the closer the ε_{eff} to the one of the air is. The guided wavelength of the structure is given by:

$$\lambda_{\text{g}} = \frac{\lambda_0}{\sqrt{\varepsilon_{\text{eff}}}} \tag{3.4}$$

Where λ_0 is the wavelength in air.

The microstrip line also has a characteristic impedance, Z_0 , which is directly dependent of the ratio w/h and the ε_{eff}. It is measured in ohms (Ω). A good approximation of it, that ignores metallization thickness, is the following [21]:

$$Z_0 = \frac{60}{\sqrt{\varepsilon_{\text{eff}}}}\ln\left(8\frac{h}{w} + 0.25\frac{w}{h}\right) \quad \text{when} \quad \frac{w}{h} < 1 \quad \text{and} \tag{3.5}$$

$$Z_0 = \frac{120\pi}{\sqrt{\varepsilon_{\text{eff}}}\left[\frac{w}{h} + 1.393 + \frac{2}{3}\ln\left(\frac{w}{h}+1.444\right)\right]} \quad \text{when} \quad \frac{w}{h} > 1 \tag{3.6}$$

As aforestated, in Figure 3.2, most of the electric field density is allocated between the strip and the ground, with a part of the electric field that goes outside the strip, also known as fringing field. Moreover, the magnetic field is coiling around the strip. This distribution of the electromagnetic field gives the possibility to excite both S-SRRs and S-CSRRs.

For the investigations regarding coupling with S-SRRs and S-CSRRs, a microstrip line with the characteristics displayed in Table 3.1 is considered.

h (mm)	**Substrate**	**w** (mm)	**t** (μm)	**Length** (mm)	**Separation x** (mm)
0.5	RO3004C ($\varepsilon_{\text{r}} = 3.38$)	1.14	17	30	0.150

Table 3.1: Microstrip, design parameters

3.2.2 Coupling with S-SRR

As described in Chapter 2, the excitation of the S-SRR is achieved by coupling it to an axial magnetic field to the ring. From Figure 3.2, the only manner to accomplish this is to locate the S-SRR on the top of the substrate, in the region which is not occupied with the strip. This makes the inherent magnetic field of the microstrip line axial to the ring, thus obtaining the desired excitation. In this structure, there are three parameters that have an influence on the coupling:

- The height of the substrate h.
- The distance to the strip x.
- The angle θ of the gap regarding the strip.

The resonators were designed with resonance frequency of 5 GHz, 10 GHz and 15 GHz and located in the vicinity of the strip. Their design parameters are summarized on Table 3.2. Their gap was allocated in the same direction of the strip, as presented on Figure 3.3 a), b) and c) ,which are the designed resonators to work at 5 GHz, 10 GHz and 15 GHz, respectively .

Radius (mm)	**Height** (mm)	**Ring Thickness** (mm)	**Gap Width** (mm)	f_0 (GHz)
3.2	0.017	0.5	0.65	5.1
1.75	0.017	0.5	0.5	10.05
1.2	0.017	0.35	0.25	15

Table 3.2: Microstrip, design parameters of the three S-SRRs

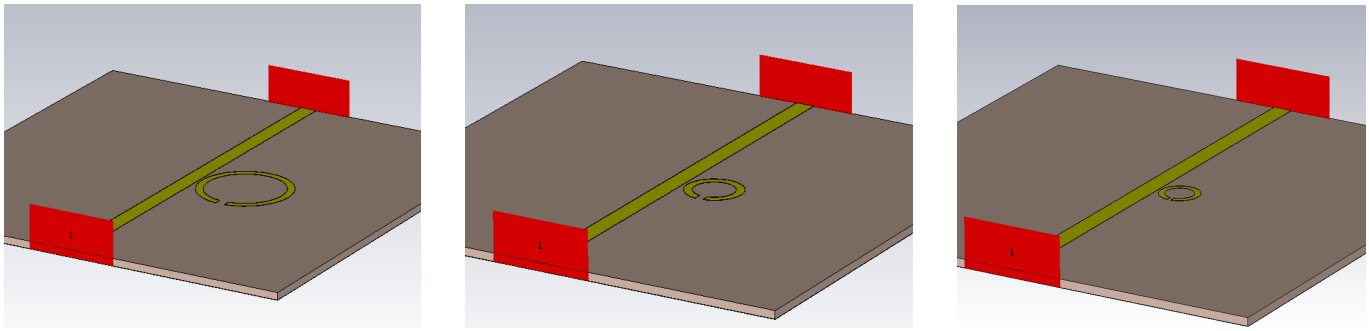

(a) S-SRR with resonance near 5 GHz (b) S-SRR with resonance near 10 GHz (c) S-SRR with resonance near 15 GHz

Figure 3.3: Microstrip, designed S-SRR to study coupling

Influence of substrate height

For the S-SRR with a large substrate height, the coupling becomes better. This is caused directly by the amount of fringing fields outside of the structure. As stated before, when the relation w/h decreases, the density of the electromagnetic field outside the structure increases, which makes the magnetic field coupling to the resonator stronger. However, as the strip and the ground are separated from each other, there is a height when the ground does not influence the field generated in the strip anymore. This is directly dependent of the penetration depth of the frequencies. Higher frequencies have lower field penetration. Therefore, for a certain height the coupling between the microstrip and the S-SRR is bound to be worse than for heights which are smaller. This critical substrate height value is lower the higher the resonance frequency is.

In order to study this parameter, seven heights between 0.1 mm and 3 mm have been considered. The results are displayed in Figure 3.4. From it, the previous statements are confirmed. At the beginning the coupling increases for higher substrate heights. Moreover, there is a certain value for each resonator where it starts to decrease. This critical substrate height is smaller for higher frequencies.

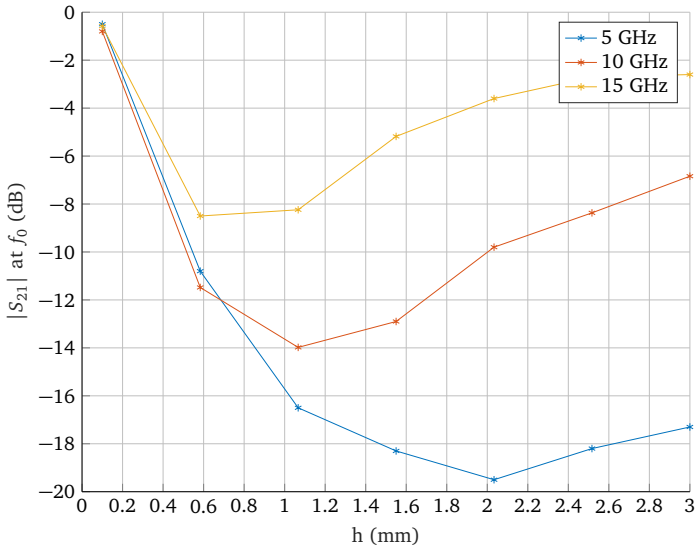

Figure 3.4: Microstrip, influence of substrate height in coupling with S-SRRs

Influence of distance from strip

Since the magnetic field is coiling around the strip, its value is higher in the vicinities of it. Consequently, the further away from the strip the resonator is, the lower the coupling. Several simulations were performed in order to prove this point, by varying the distance between the strip and the resonator from 0.05 mm to 1 mm. The results on Figure 3.5 confirm the previous affirmation. It can be seen that for wider separations between both structures the coupling becomes weaker. Furthermore, for separations larger than 0.8 mm the coupling is almost negligible.

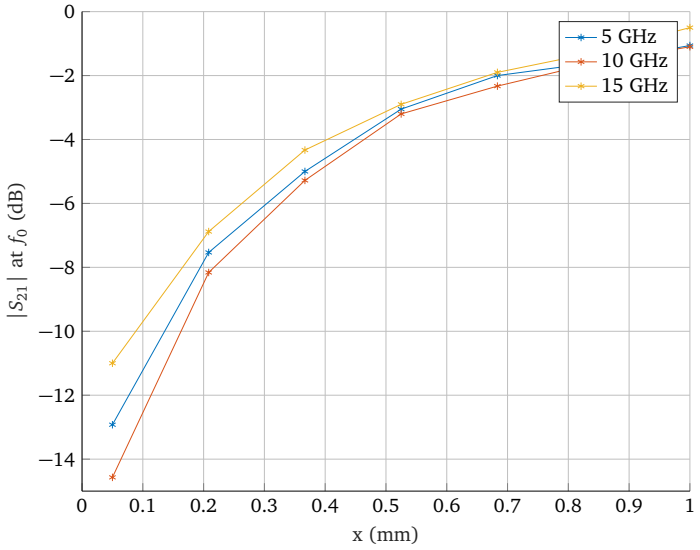

Figure 3.5: Microstrip, influence of distance strip - S-SRR in coupling

Influence of angle θ of the gap regarding the strip

The magnetic field density value changes along the resonator. This has a direct influence in the excitation of the S-SRR. Hence, the highest coupling is achieved when the gap of the resonator is as far as possible away from the strip, since this structure allows the magnetic field with highest value to be coupled into it. To confirm this with empirical evidence, five simulations for $\theta = 0°$, $45°$, $90°$, $135°$ and $180°$ are performed. Before performing the simulations, the resonators in Figure 3.3 are rotated 90° clockwise, so the gap is orthogonal to the strip and in the side of the ring which is nearest it. For $\theta = 180°$, the gap is in the opposite place of the ring. Thus, being as far as possible away from the strip. Figure 3.6 confirms the previous statement. As the gap gets farther from the strip, the coupling increases.

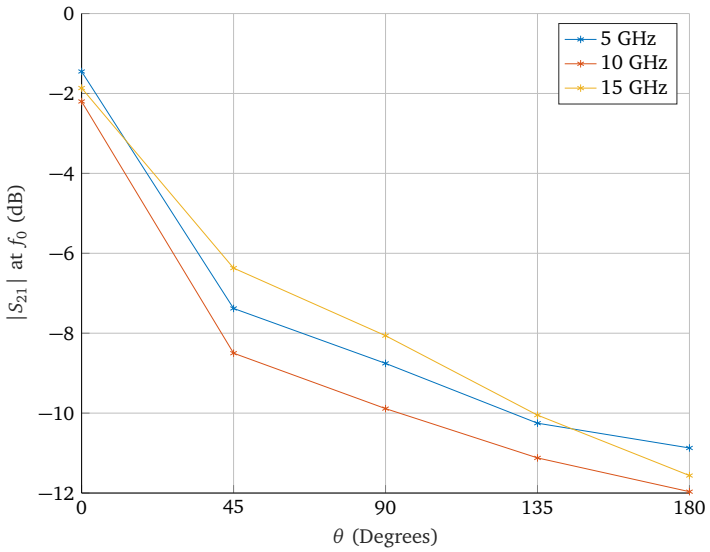

Figure 3.6: Microstrip, influence of the angle θ in coupling with S-SRRs

3.2.3 Coupling with S-CSRR

As aforestated in Chapter 2, the excitation of the S-CSRR is achieved by coupling it to an axial electric field to the ring. From Figure 3.2, there are two possibilities for the EM field of a microstrip line where this can be achieved. On the one hand, the S-CSRR can be placed on the strip of the line. However, this disrupts the fundamental mode of the microstrip, which arises problems. For instance, the excitation for resonators located after the first one is not given. On the other hand, the structure can be placed on the ground of the microstrip and directly below the strip, where the E field density is maximum. With this approach, a proper coupling between S-CSRRs and the microstrip line can be achieved.

For this structure, there are two parameters that have a high influence on the coupling, that are:

- The height of the substrate h.
- The angle of the gap regarding the strip.

The design parameters of the three selected resonators working at 5, 10 and 15 GHz are displayed on Table 3.3. Figure 3.7 a), b) and c) shows the three resonators devised with CST. The red lines are the outline for the strip, in the upper part of the structure.

Radius (mm)	**Height** (mm)	**Ring Thickness** (mm)	**Gap Width** (mm)	f_0 (GHz)
3.6	0.017	0.5	0.65	5.01
2	0.017	0.5	0.65	9.885
1.25	0.017	0.35	0.35	15.16

Table 3.3: Microstrip, design parameters of the three S-CSRRs

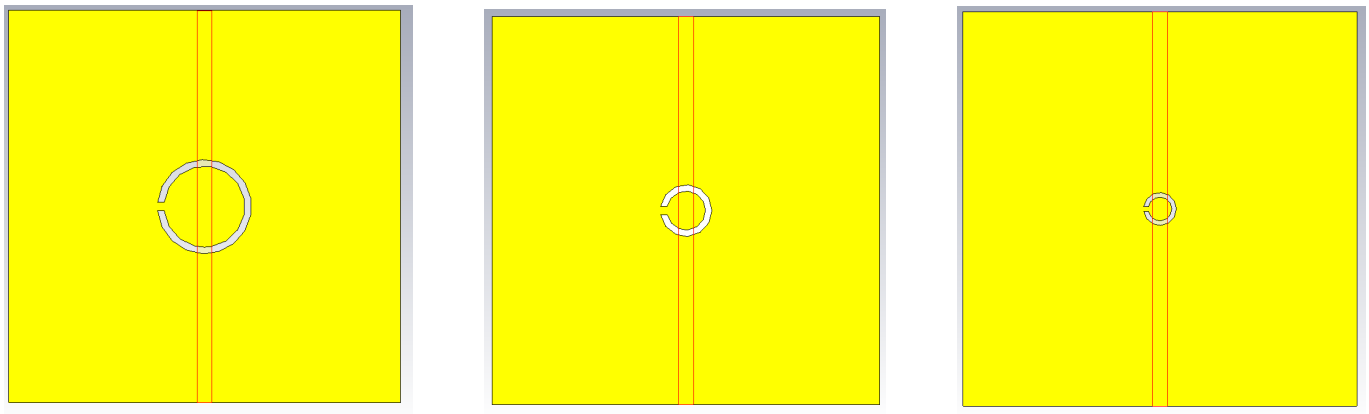

(a) S-SRR with resonance near 5 GHz (b) S-SRR with resonance near 10 GHz (c) S-SRR with resonance near 15 GHz

Figure 3.7: Microstrip, designed S-SRRs to study coupling

Influence of substrate height

As it was stated in Section 3.2.1, when the relation w/h is large enough, the microstrip line behaves as a parallel plate capacitor, with a large part of the electric field density between the strip and the ground of the line. This is exactly the field direction needed in order to excite the S-CSRRs. Due to this, for large substrate heights the coupling decreases.

In Figure 3.8, simulations results with different substrate heights between 0.1 mm and 3 mm are displayed. The results confirm the previous statement. Moreover, the coupling is better for lower frequencies. This can be understood in term of the penetration depth in the substrate associated with each frequency. Since this value inversely proportional to the frequency, the coupling between the strip and resonator is less affected by the increase of the substrate height for lower resonance frequencies.

Influence of angle θ of the gap regarding the strip

The gap in the resonators of Figure 3.7 is located orthogonally regarding the strip. In other words, the gap is parallel to the inherent electric field of the microstrip line. This, as it was explained in Section 2.2, makes the influence of the electric incident field smaller. When the resonator is rotated, the coupling between it and the field is increased, until it reaches a maximum value when the gap and the field are aligned orthogonally. This happens when the gap and the strip are parallel regarding each other. Thus, a maximum peak in the coupling is expected for $\theta = 90^o$, where θ is the angle of the rotation regarding the previously presented resonators. The coupling for different angles is displayed in Figure 3.9, where this peak at the aforemetioned angle is easily seen.

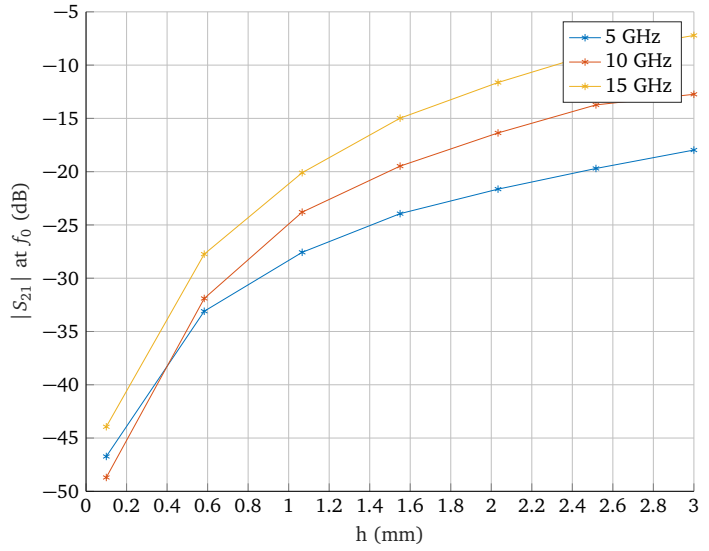

Figure 3.8: Microstrip, influence of substrate height in coupling with S-CSRRs

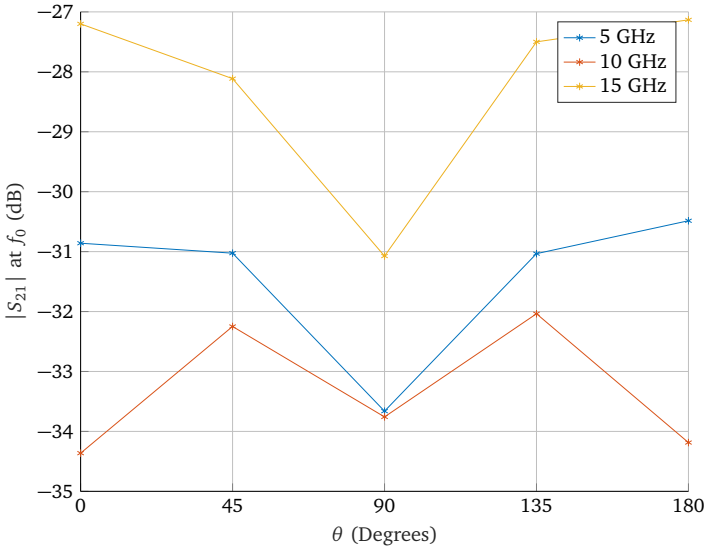

Figure 3.9: Microstrip, influence of the gap angle in coupling with S-CSRRs

3.3 The Coplanar Waveguide

The coplanar waveguide (CPW) was firstly presented by C.P. Wen in 1969 in [23]. Although not as famous as the microstrip lines, they are nevertheless widely used in several RF and microwave applications. Like the microstrip line, their nature is planar, which allows an easy fabrication and circuit integration. Furthermore, high frequency signals up to 100 GHz can be transported along the line, since there are no parasitic discontinuities in the ground plane of the structure. However, they potentially present more losses compared to the microstrip line, depending mostly of their substrate thickness.

3.3.1 Definition

Coplanar Waveguides are formed by a substrate, in whose upper part a central strip of width w is located. The ground of the structure is also in this plane, at both sides of the central strip and separated a distance g from it. Although there is the possibility to have a ground in the bottom part of the substrate, resulting

in a structure called Grounded Coplanar Waveguide, in this bachelor thesis only the former structure is considered. Figure 3.10 displays the basic layout of a CPW.

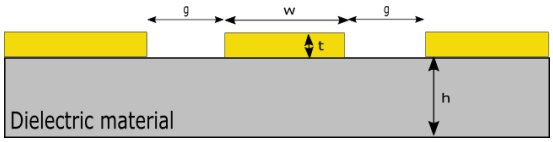

Figure 3.10: Coplanar waveguide layout

For such a transmission line, its inherent electromagnetic field propagates inside and outside the substrate. The electric field is generated between the central strip and the ground planes of its sides. The magnetic field is mostly coiling around the central strip, as well as it presents a small part of it twirling around the ground planes. Figure 3.11 shows a sketch of this EM field.

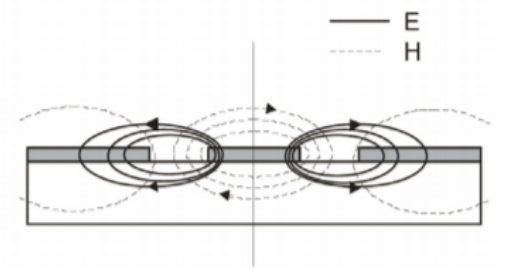

Figure 3.11: Coplanar waveguide, sketch of EM field from [26]

As it is seen before, the electromagnetic field of the CPW propagates outside the substrate. This means that the signals into it experiment a dispersion effect, just like the microstrip line. When the substrate height of the CPW is thick enough, its effective permittivity for the line surrounded by air can be calculated as:

$$\varepsilon_{\text{eff}} = \frac{\varepsilon_{\text{r}} + \varepsilon_{\text{air}}}{2} , \tag{3.7}$$

where ε_{r} is the relative permittivity of the substrate, and ε_{air} the one from the air, whose value is always 1. However, this expression is inaccurate for thin coplanar waveguides. In order to find their exact value, conformal-mapping based analytic formulas have been investigated over the last years, such as presented in [24] .

The characteristic impedance of a coplanar waveguide depends on the strip width, gap width, metallic thickness and substrate height. However, in order to find an exact expression for it conformal mapping must be applied. An expression for its impedance, found in [25] is:

$$Z_0 = \frac{30\pi}{\sqrt{\varepsilon_{\text{eff}}}} \frac{K'(k_1)}{K(k_1)} , \tag{3.8}$$

where K and K' represent the complete elliptic integral of the first kind and its complement, and k_1:

$$k_1 = \frac{w}{w + 2g} \tag{3.9}$$

Furthermore, when the CPW is to be designed to match a certain impedance, its design parameters have an infinity set of solutions. Thus, an easy form to decide its values is to use coplanar waveguide calculators, such as the ones offered by Microwave Office or CST Studio.

The EM field displayed in Figure 3.11 gives the possibility to couple S-SRRs and S-CSRRs to the CPW. For the investigations regarding this coupling, a CPW with the characteristics presented in Table 3.4 is considered.

h (mm)	**Substrate**	**w** (mm)	**g** (mm)	**t** (μm)	**Length** (mm)	**Separation x** (mm)
0.5	RO3004C ($\varepsilon_r = 3.38$)	6	1	17	30	0.150

Table 3.4: CPW, design parameters

3.3.2 Coupling with S-SRR

In order to obtain an axial magnetic field to the S-SRR,the resonators are placed in the bottom of the substrate of the CPW. Thus, the magnetic field that gets pulled into the substrate couples and excites the resonators. When the structure is placed exactly below the gaps of the CPW, the magnetic field coupling into it is maximum. The excitation of the resonator is mainly influenced by three factors:

- The width of the gap between the central strip and the ground g.
- The height of the substrate h.
- The angle of the resonator split regarding the central strip θ.

The resonators were designed to have resonance frequencies near 5 GHz, 10 GHz and 15 GHz. The final structures parameters are shown on Table 3.5. Also, Figure 3.12 a), b) and c) present these three structures.

Radius (mm)	**Height** (mm)	**Ring Thickness** (mm)	**Gap Width** (mm)	f_0 (GHz)
3.3	0.017	0.5	0.65	5.01
1.75	0.017	0.35	0.5	9.9
1.35	0.017	0.5	0.65	15.35

Table 3.5: CPW, design parameters of the three S-SRRs

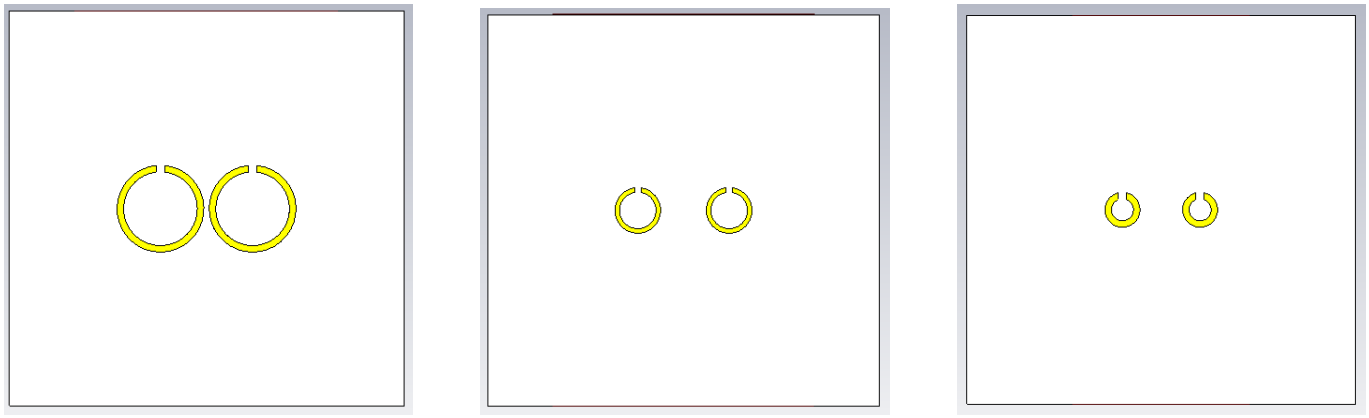

(a) S-SRR with resonance near 5 GHz (b) S-SRR with resonance near 10 GHz (c) S-SRR with resonance near 15 GHz

Figure 3.12: CPW, designed S-SRRs to study coupling

Influence of gap width between strip and ground g

On the one hand, the increase of the distance between the central strip and the ground does not affect highly the magnetic field along the resonator, as most of it is coiling around the central strip. Thus, the S-SRR is excited regardless the distance between the components on the top of the substrate.

On the other hand, in Figure 3.13 the effect in the coupling is displayed for different distances. It is seen that, although the resonator is being excited, the larger the distance between the ground and the strip is, the less excitation achieved. This is due to how the S-SRRs are set in the simulation on CST. They are forced to be always in the middle of the gap, regardless its size. Thus, when the gap is increased, they are separated from the coplanar. Since the magnetic field is mostly coiling around the central strip, the excitation that they suffer is smaller. Moreover, the structure with resonance at 5 GHz presents a larger coupling than the other two. This is a direct effect of its size. This resonator has a larger radius than the other two, so it occupies more space below the central strip. Thus achieving a higher coupling to the magnetic field of the CPW.

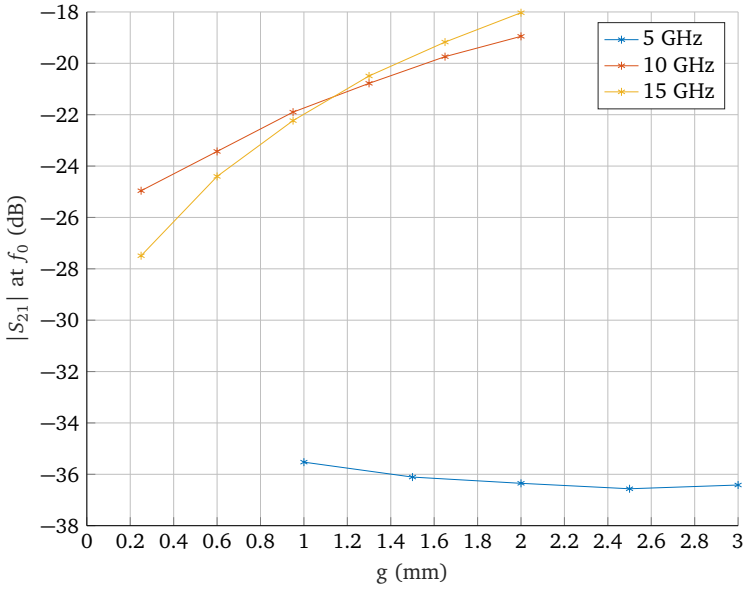

Figure 3.13: CPW, influence of gap width on coupling with S-SRR

Influence of substrate height h

When the thickness of the substrate is increased, more electric field gets pulled into it. Although the magnetic field density inside the substrate also grows, it is mostly concentrated in the region below the central strip, whereas the resonators are located on the bottom of the substrate. Consequently, as the substrate height increases, the resonators are separated further from the strip, which makes the excitation that they receive smaller. Thus, the value of $|S_{21}|$ at the resonance frequency is decreased.

Figure 3.14 displays the aforementioned peak for different substrate heights between 0.1 mm and 3 mm. As stated, the amplitude of the peak is smaller for a larger substrate thickness.

Influence of angle θ of the resonator gap regarding the strip

The location of the gap in the ring determines the influence of the tangential electric field that is coupling to the resonator. When the aforemetioned gap is located orthogonally to the electric field its coupling is as high as possible. In other words, when it is parallel to the CPW gaps. Examples of such structures are displayed in Figure 3.12. Thus, a minimum peak amplitude is expected for this angle.

In Figure 3.15 the coupling is presented for different rotations of the ring. The starting parameter set is the gaps of both resonators located in front of each other. Then, the rotation angle is swept between 0° and 180°. The previous statement is confirmed, there is a higher coupling for $\theta = 90°$. The smaller value for 0° is due to the coupling between the electric fields of the resonators, as their gaps are in front of each other.

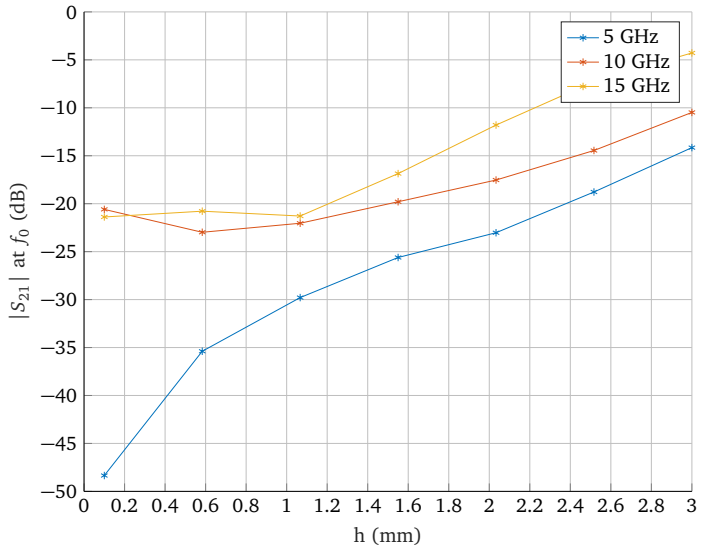

Figure 3.14: CPW, influence of substrate height in coupling with S-SRR

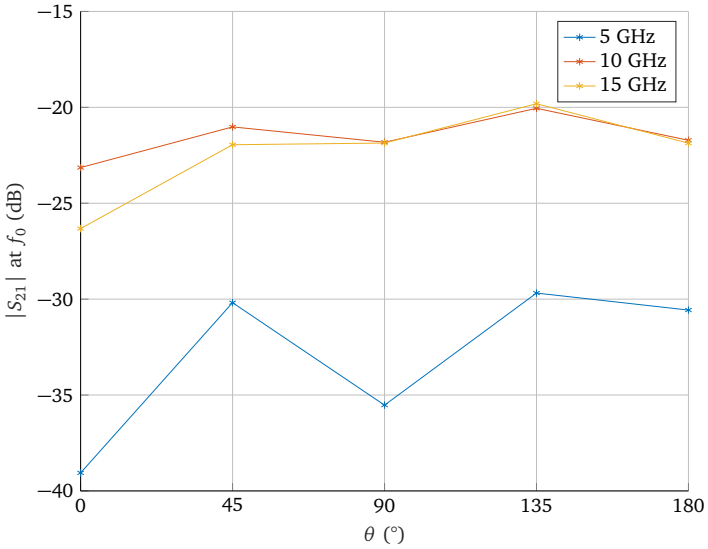

Figure 3.15: CPW, influence of S-SRR angle on coupling

3.3.3 Coupling with S-CSRR

The S-CSRR is excited by an axial electric field to the ring. In the CPW, and in light of the electric field presented in Figure 3.11, there are two possible positions where the S-CSRR can be allocated. On the one hand, it can be excited by placing it in the middle of the central strip. However, this disturbs the fundamental mode of the transmission line, which leads to an unpredictable behaviour of other devices after the resonator. On the other hand, the S-CSRRs can be situated in the ground planes of the coplanar waveguide. This way, they are coupled to the electric field of the line. In this situation, there are four factors that affect the excitation of the resonators.

- The width of the gap between the central strip and the ground g.
- The height of the substrate h.
- The separation between the resonators and the gap x.
- The angle of the resonator gap regarding the central strip θ.

In order to study the aforementioned parameters, the resonators were designed to work at 5 GHz, 10 GHz and 15 GHz, with the parameters presented in table 3.6. The CPW design is the same as the previous section, with its parameters displayed in Table 3.4. In addition, Figure 3.16 displays the layout of the three structures used for the simulations.

Radius (mm)	**Height** (mm)	**Ring Thickness** (mm)	**Gap Width** (mm)	f_0 (GHz)
3.8	0.017	0.5	0.65	5.01
1.95	0.017	0.35	0.65	9.96
1.3	0.017	0.4	0.25	15.025

Table 3.6: CPW, design parameters of the three S-CSRRs

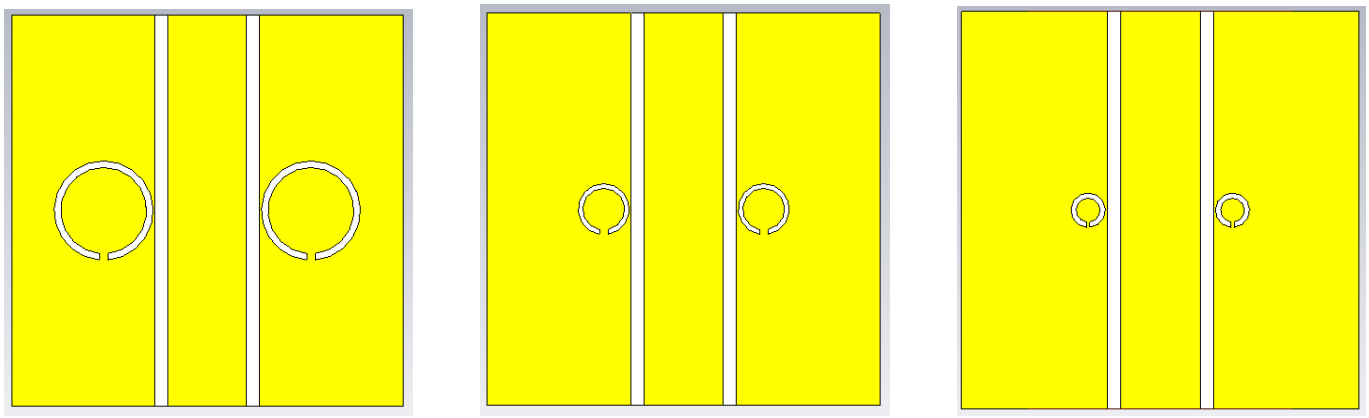

(a) S-SRR with resonance near 5 GHz (b) S-SRR with resonance near 10 GHz (c) S-SRR with resonance near 15 GHz

Figure 3.16: CPW, designed S-CSRRs to study coupling

Influence of gap width between strip and ground g

As the separation between the ground and the central strip increases, the electric field density at the ground plane decreases. Moreover, the excitation of the S-CSRRs depends directly on this field. Thus, the excitation achieved as well as the coupling to the CPW are smaller the higher this distance is. Figure 3.17 confirms this statement. The curves have a tendency to grow, which indicates a decrease in the coupling of the structure.

Influence of substrate height h

The excitation of the resonator when varying the substrate thickness depends mainly of two factors. The amount of electric field stored in the substrate and the penetration depth at the resonance frequency.

As the substrate height increases, the electric field energy stored into it is larger. Since the resonators are excited by this field, their coupling strength grows. A further effect of an increasing substrate height is that the electric field is scattered along the substrate, which in turn means that less field is coupled to the resonators. Thus, there is a certain height for which the coupling decreases.

In Figure 3.18, simulation results for substrate heights between 0.1 mm and 3 mm are displayed. The resonator at 5 GHz has a higher coupling than the other two, due to having a larger size. This allows more electric field to be coupled into it. Moreover, the critical substrate height is reached before for the S-CSRR whose resonance frequency is 15 GHz, for a substrate thickness around 1 mm.

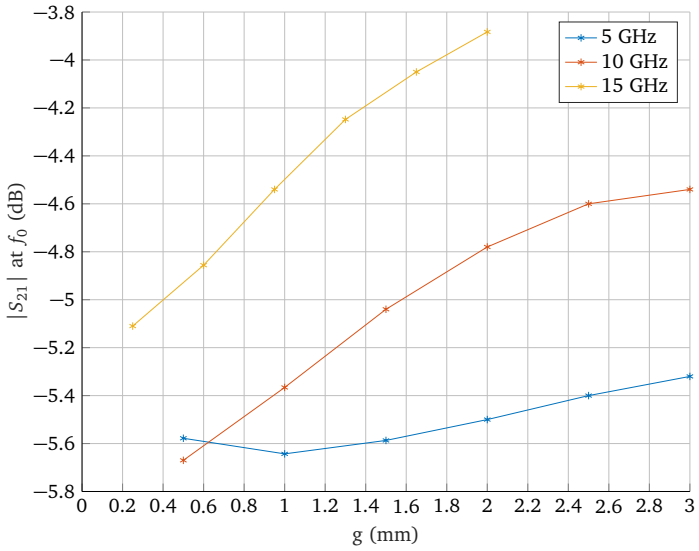

Figure 3.17: CPW, influence of gap width on coupling with S-CSRR

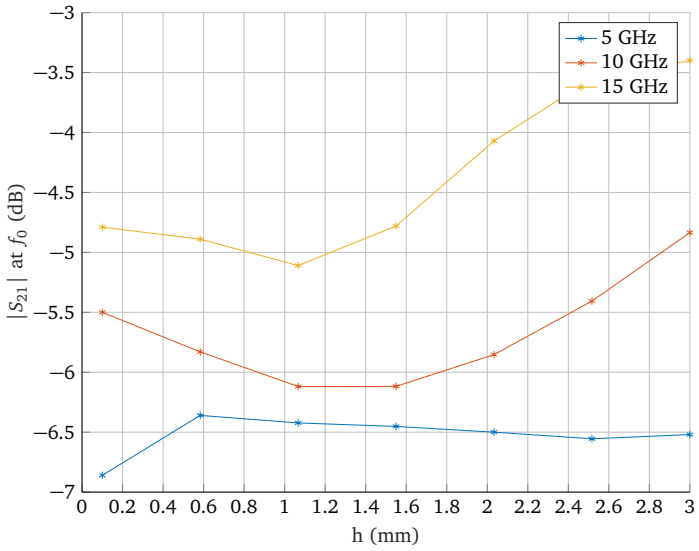

Figure 3.18: CPW, influence of substrate height on coupling with S-CSRR

Influence of separation between S-CSRR and CPW gap x

When the resonators are shifted from near the gap to far from it, the coupled electric field density decreases. This in turn means that the excitation strength in the resonator is smaller, thus decreasing amplitude the peak of the $|S_{21}|$ at resonance. In Figure 3.19 this effect is appreciable. The larger the separation between the resonator and the gap of the CPW, the lower the coupling between the transmission line and the S-CSRRs.

Influence of angle θ of the resonator gap regarding the strip

As the resonators are located on the ground of the CPW, the electric field value is not constant along them, but it is higher in the vicinities of the CPW gap. Therefore, the highest coupling possible is achieved when the metallic gap of the resonator is as far as possible from the strip, since this structure allows more electric field to be coupled to it. Figure 3.20 displays the results obtained from the simulations. The lower coupling for 90° and 135 ° might be due to a destructive interference that happens only at 5 GHz between the field of the resonator and the field of the transmission line.

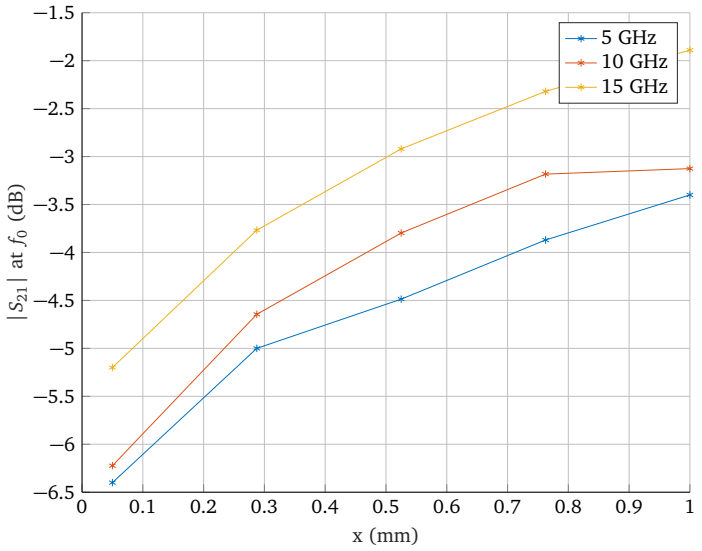

Figure 3.19: CPW, influence of separation of S-CSRR regarding the CPW gap

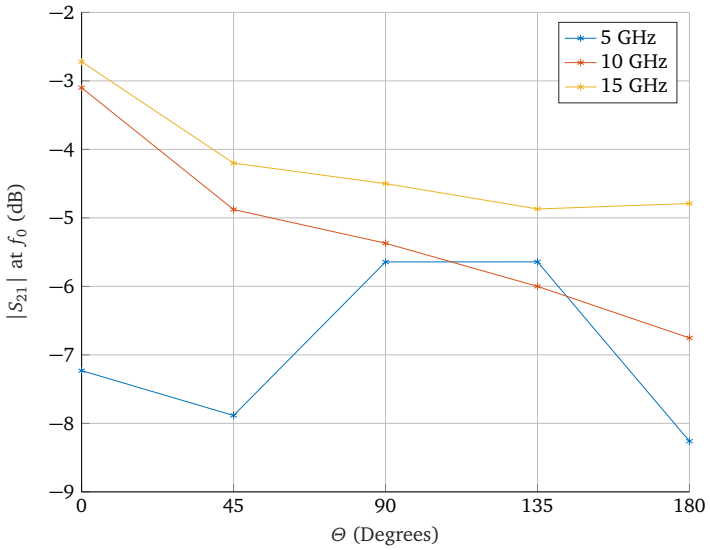

Figure 3.20: CPW, influence of S-CSRR angle on coupling

4 Sensitivity Analysis of Resonators

The sensitivity is defined as the accuracy to distinguish the materials that are being analysed. The main challenge regarding the detection of healthy and malignant tissue is to determine the differences between the dielectric permittivity of them. Moreover, this problem has an extra difficulty, as they both have a large ε_r. Thus, it is necessary to pay great attention to the sensitivity of the resonators, as well as develop an enhanced structure to optimize it.

During this Chapter, a figure of merit regarding the sensitivity is given and evaluated. The structures presented in Chapter 3 are evaluated and optimized in function of their frequency shift when loaded with a material of $\varepsilon_r = 2$. Then, the most suitable structure is chosen by applying the aforestated figure of merit, whose suitability to evaluate different resonators is also addressed.

4.1 Definition

When a dielectric is placed in the top of a unloaded resonator, the resonance frequency of the system is shifted towards lower values. The higher the dielectric permittivity of the dielectric, the larger the distributed capacitance of the system is. Thus, the shift in the resonance frequency is also more substantial. Consequently, the new resonance of the structure can be calculated as:

$$f_{0,\text{new}} = \frac{1}{2\pi\sqrt{L_{\text{res}}(C_{\text{res}} + C_{\text{dilec}})}} \tag{4.1}$$

Where L_{res} and C_{res} are the inductance and capacitance of the resonator, and C_{dilec} the capacitance caused by the material used to load the resonator.

Since each material has a different ε_r, the shift of the resonance frequency caused by them is different. For instance, the permittivity of ex vivo malignant liver tissue is between 19% to 30% larger than that of healthy tissue [27]. Although this value seems to be sufficiently large, being able to detect this shift accurately is by no means a trivial task, specially for large relative permittivity values, such as the human body tissue. The relative frequency shift is given by:

$$\Delta f / f_0 = \frac{f_{0,\text{ old}} - f_{0,\text{ new}}}{f_{0,\text{ old}}} \tag{4.2}$$

With this definition and for this bachelor thesis, its value is always positive, since the new resonance frequencies are compared with the resonance frequency of the resonator when surrounded by air, as it is displayed in Figure 4.1.

If Equation (4.2) is further developed by inserting into it Equation 4.1, it turns out that the relative shift can be calculated in function of the capacitances of the structure:

$$\Delta f / f_0 = \frac{\frac{1}{2\pi\sqrt{L_{\text{res}}C_{\text{res}}}} - \frac{1}{2\pi\sqrt{L_{\text{res}}(C_{\text{res}}+C_{\text{dilec}})}}}{\frac{1}{2\pi\sqrt{L_{\text{res}}C_{\text{res}}}}} = 1 - \frac{\sqrt{C_{\text{res}}}}{\sqrt{C_{\text{res}} + C_{\text{dilec}}}} \tag{4.3}$$

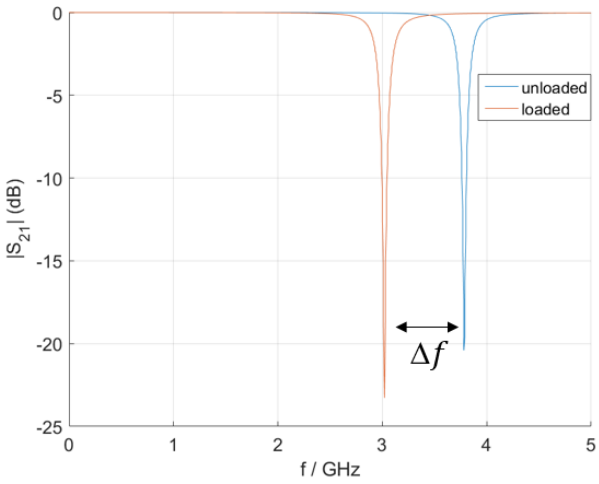

Figure 4.1: Frequency shift for a loaded resonator

A straightforward conclusion from this equation is that the sensitivity is always a value between 0, when there is no shift, and 1, when $C_{\text{res}} \rightarrow \infty$. Moreover, from this equation it is possible to see the reason about why it is difficult to successfully distinguish between two materials with high ε_{r}. The higher their dielectric permittivity, the larger the distributed capacitance that they add to the system. For instance, if C_{res} is considered to have a certain value, and the relative shift in frequency is calculated for C_{dilec} between 0 and 100, the result is displayed on Figure 4.2.

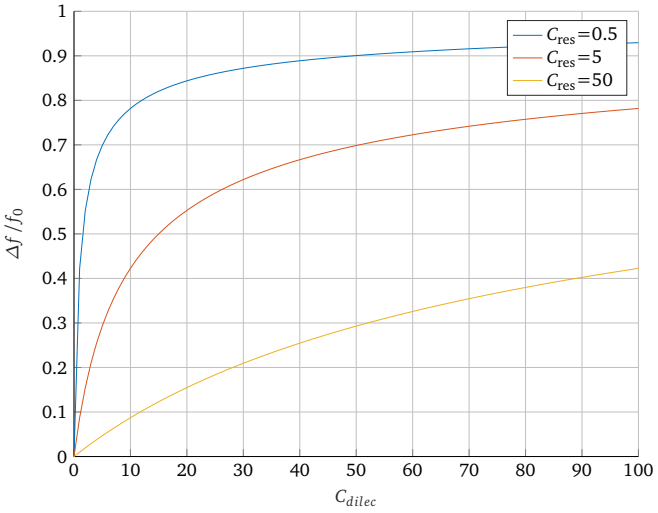

Figure 4.2: $\Delta f / f_0$ for different values of C_{dilec}

From Figure 4.2, it can be seen that for higher values of C_{res} the relative shift of the resonance frequency is larger when measuring higher permittivity materials. Moreover, a low C_{res} makes the task to distinguish between materials with low ε_{r} easier. Thus, the optimization of this value plays an important role in the sensitivity. In this bachelor thesis, this optimization is studied for design parameters of unloaded S-SRRs and S-CSRRs when loading them with a lossless material of $\varepsilon_{\text{r}} = 2$.

Although the relative shift is important to evaluate the sensitivity, is not the only factor that plays a role into it. The identification of a proper resonance frequency is crucial to be able to calculate the aforementioned shift. For instance, if the bandwidth at resonance is extremely broad, the task to determine the resonance frequency gets more difficult. Due to this, a Figure of Merit (FoM) is defined. It takes into account the rela-

tive frequency shift and the sharpness of the resonance peak, represented by the normalized -1dB bandwidth B_{1dB}/f_0.

$$\text{FoM} = \frac{\Delta f}{B_{1dB}} \tag{4.4}$$

In the following sections, the relative frequency shift is studied and optimized for the structures described in Chapter 3. From them, the four structures that have the larger frequency shift are chosen, and the most suitable in terms of sensitivity is selected by using the FoM.

4.2 Relative frequency shift in transmission lines

The shift in the resonance frequency is highly dependent on the electric field distribution of the resonators. As they are being loaded with dielectric blocks whose relative permeability μ_r is 1, the magnetic field value is not modified. However, those dielectric blocks also have a relative permittivity ε_r higher from ε_{air}. The larger the value that the electric field previously had, the broader the shift experimented when loading the resonator.

Following this argument, S-CSRRs experiments a larger resonance shift than S-SRRs. For these resonators, the sensitive area is located between the two sides of the ring, whereas for S-SRRs it is in the gap of the resonator. Thus, its sensing surface is larger. During this section, this is seen in every result. Moreover, which design parameters of the resonator affect the frequency shift and how they increase or decrease it is discussed.

The studied structures are the ones presented in Chapter 3, with three different substrate heights of 0.127 mm, 0.254 mm and 0.5 mm. In order to give more insight about the difference in the resonance shift between both types of resonators, the results are presented together. For the S-SRR in the microstrip and the C-SRR in the CPW, the distance respect the strip and the gaps is set to 0.150 mm, respectively. This value is chosen because it gives a sufficiently high coupling and is large enough to be fabricated without inaccuracies. The substrate used is Rogers RO3004C and the metallization has a thickness of 0.017 mm. The design parameters of the transmission lines are chosen to have a characteristic impedance of 50 Ω, when possible.

For the different structures, the parameters that are evaluated to maximize the frequency shift are:

- The substrate height h.
- The angle θ of the resonator regarding the transmission line.
- The resonator width w.
- The gap width g.

4.2.1 Microstrip line

As aforestated, one of the conditions is that the characteristic impedance of the line has to be 50 Ω.This means that for each height the strip width must be adjusted in order to accomplish this condition. The calculated values are presented in Table 4.1.

The S-SRRs and S-CSRRs have the design parameters presented in Tables 3.2 and 3.3, respectively.

h (mm)	**w** (mm)	Z_0 (Ω) (f =5 GHz)	Z_0 (Ω) (f =10 GHz)	Z_0 (Ω) (f =15 GHz)
0.127	0.28	49.89	49.83	49.8
0.254	0.57	50.02	49.99	50.01
0.5	1.14	49.92	50.00	50.25

Table 4.1: Microstrip, design parameters for Z_0 = 50 Ω

Influence of substrate height

The thickness of the substrate, as explained in Section 3.2, has a direct influence in the coupling between the microstrip line and the resonators. For the S-SRR, the coupling improves until one certain value, whereas for the S-CSRR to increase the substrate height leads to less coupling. For the relative resonance shift, the tendency is the same. When the coupling of the resonators is stronger, their electric field amplitude is also higher. Thus, when loading the resonator with a dielectric block, the relative shift is larger. In Figure 4.3 a) and b) the frequency shift for the three S-SRR and S-CSRR for the three aforementioned heights is displayed, respectively.

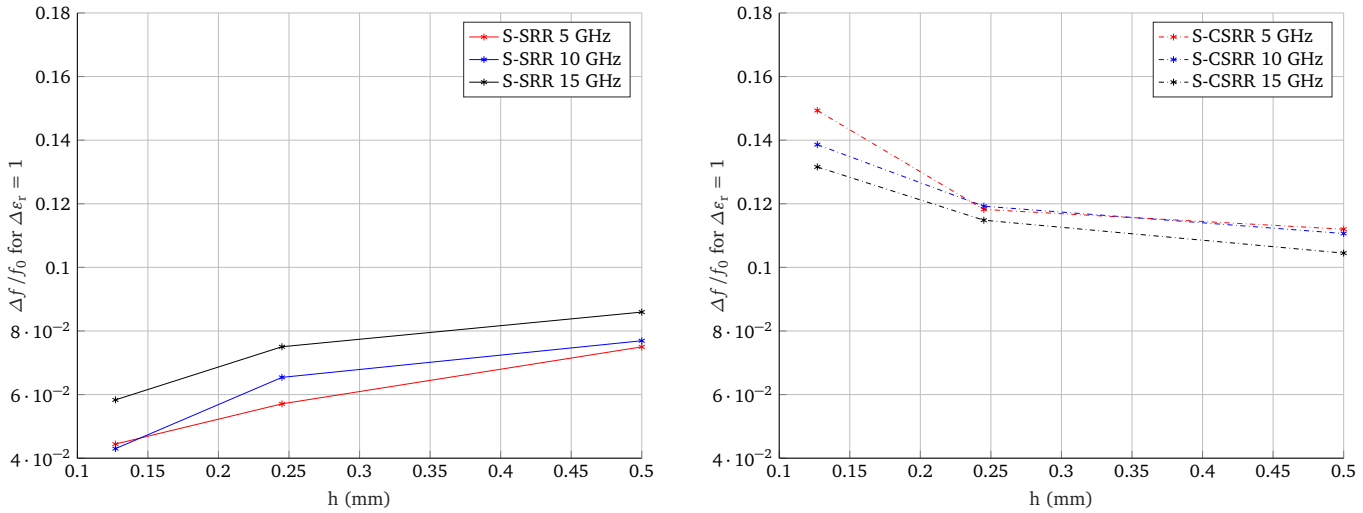

(a) S-SRR, $\Delta f / f_0$ vs substrate height

(b) S-CSRR, $\Delta f / f_0$ vs substrate height

Figure 4.3: Microstrip, $\Delta f / f_0$ in dependency of substrate height

From Figure 4.3, it can be seen that the highest relative frequency shift is achieved in the S-SRR for a substrate height of 0.5 mm with operating frequency of 15 GHz. In contrast, the S-CSRR perform best for a height of 0.127 mm and at resonance of 5 GHz.

On the one hand, for the S-CSRR this is the configuration that brings the highest coupling possible. Thus, as expected, the shift is the largest. On the other hand, for the S-SRR this configuration achieves minimum coupling, in regards to the other studied heights and frequencies. When the structures are loaded with a dielectric block, their electric field is redirected by it. This modification causes a discharge of the resonators with resonance at 10 GHz and 15 GHz though the transmission line. The field that is generated by being coupled to the microstrip is also coupling backwards to the strip of the line. Consequently, the two structures that are further analysed are the S-SRR with resonance frequency of 15 GHz and substrate height of 0.5 mm and the S-CSRR whose resonance is in 5 GHz and substrate height of 0.127 mm.

Another important phenomenon that can be seen when both performances are compared, is that the S-CSRR presents a larger shift than the S-SRR. This is, as stated before, due to the S-CSRR having a larger area of sensing than the S-SRR.

Influence of θ of resonator regarding the strip

Since the behaviour of the resonators is symmetric, only half of a whole rotation of the ring is simulated. From Section 3.2, the coupling for the S-SRR is maximum when the gap is in the opposite part of the ring regarding the strip. Moreover, for the S-CSRR the coupling is maximum when the gap is in the same direction as the strip. In Figure 4.4 the frequency shift for θ between 0° and 180° is displayed.

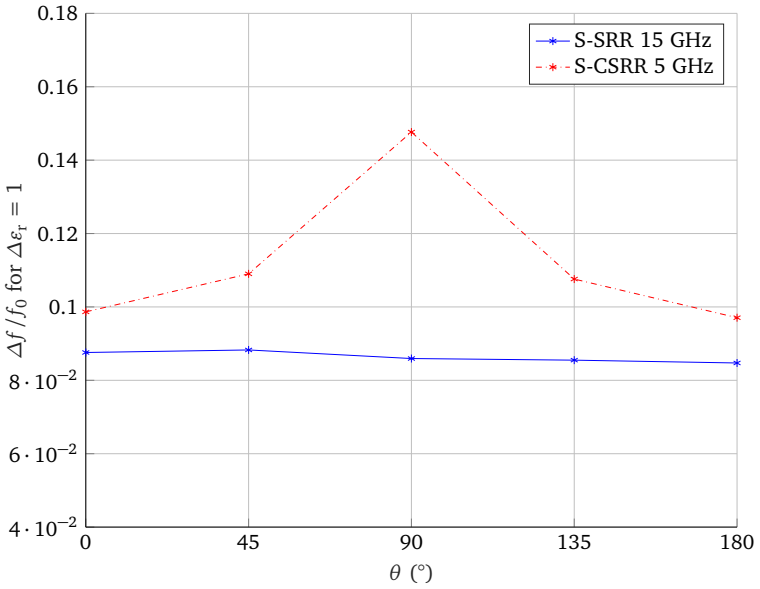

Figure 4.4: Microstrip, $\Delta f / f_0$ in dependency of θ

In Figure 4.4, the frequency shift for the S-SRR does not change significantly when rotating the ring. This is caused by the low coupling of the resonator with the microstrip, which in turns means that the electric field concentration does not experiment large variations. In comparison, the S-CSRR has a clear maximum value of frequency shift when the gap is aligned with the strip. As explained before, this increments the electric field concentration in the resonator. Thus, the shift is enhanced. Consequently, from on now the gap of the S-SRR is located with $\theta = 180°$ and the gap from the S-CSRR with $\theta = 90°$.

Influence of resonator width w

On the one hand, increasing the width of the S-SRR means that the losses of the resonator are also increased, due a larger amount of metallization in the structure. However, it also brings an increase in the electric field in the vicinities of the gap. Thus, there is a resonator width for which the frequency shift is maximum. After it is reached, the losses of the resonator predominate over the structure, so the frequency shift and the coupling decrease. This is displayed in Figure 4.5, where it can be seen that the S-SRR has a maximum relative frequency shift with w = 0.45 mm.

On the other hand, when the ring of the S-CSRR is wider its electric field amplitude decreases. Nevertheless, the coupling between the resonator and the microstrip is strong enough to guarantee an almost constant field amplitude with the ring widths that were considered. In consequence, the sensing surface of the resonator is larger while maintaining the same electric field amplitude. Moreover, the decrease of metallization also diminish the losses of the structure. Thus, for wider rings the S-CSRR presents a larger frequency shift, while the coupling is strong enough. This can be seen in Figure 4.5, although the increase in the frequency shift is almost insignificant for large ring widths. Therefore, the new width selected is 1.85 mm, since is a value for which the frequency shift and the coupling of the resonator are well-balanced

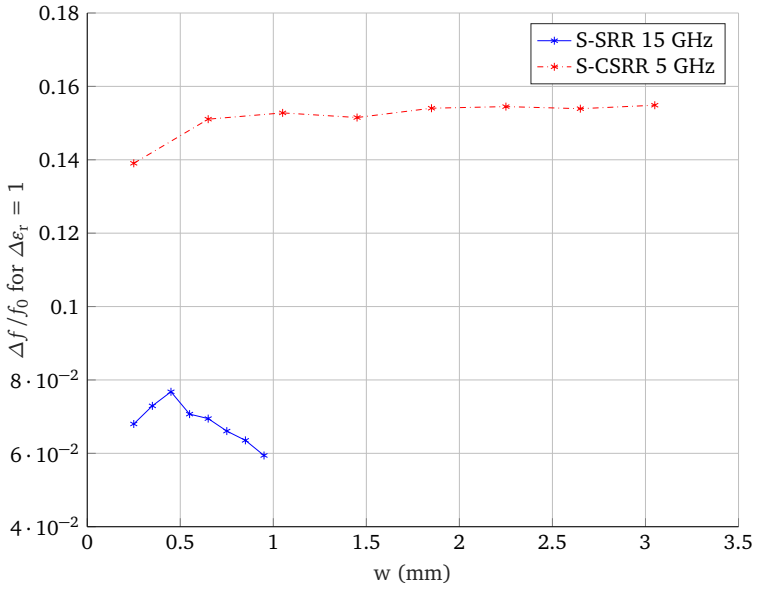

Figure 4.5: Microstrip, $\Delta f / f_0$ in dependency of width of resonator

Influence of gap width g

For the S-SRR, with increasing gap width there is a decrease of the electric field amplitude. When the gap in this resonator is considered as a parallel plate capacitor, for larger gap widths the electric field value is lower. Consequently, the frequency shift decreases. Conversely, for the S-CSRR, increasing the width of the metallic gap means a higher concentration of the electric field in the ring, for the same coupling. Thus, the frequency shift is increased.

In Figure 4.6, the Δf for different gap widths is displayed. As expected, the simulations confirm the aforestated. Henceforth, the gap width of the S-SRR is chosen to be 0.15 mm. However, for the S-CSRR a width of 1.85 mm is selected instead of the maximum one. This is owing to that the objects of study of this bachelor thesis are circular resonators, and for large values of the gap the resonator is no longer circular, but a hybrid between circular and square CSRR.

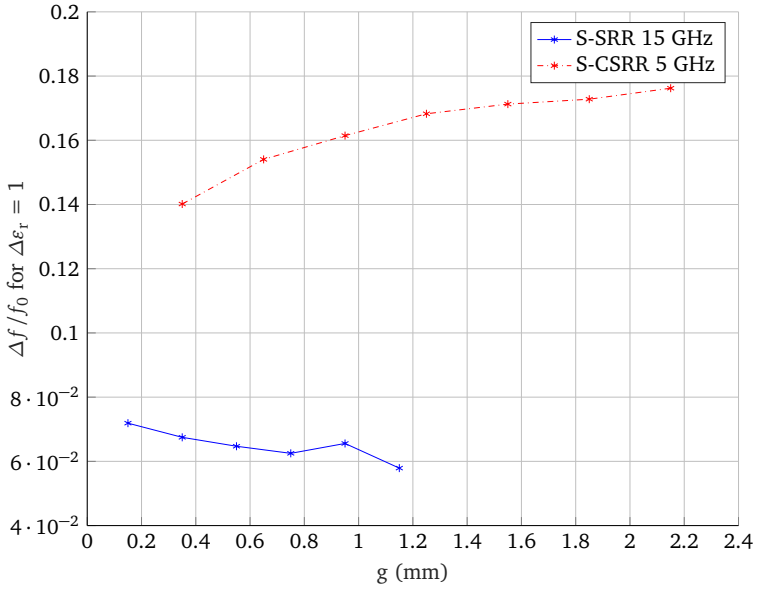

Figure 4.6: Microstrip, $\Delta f / f_0$ in dependency of width of resonator gap

4.2.2 Coplanar waveguide

As it is done for the microstrip, the design parameters of the coplanar waveguide are chosen to achieve a characteristic impedance of 50 Ω. The values for the corresponding parameters are displayed on Table 4.2.

h (mm)	**w** (mm)	**g** (mm)	Z_0 (Ω) (f =5 GHz)	Z_0 (Ω) (f =10 GHz)	Z_0 (Ω) (f =15 GHz)
0.127	6	0.22	49.89	49.83	49.8
0.254	6	0.26	50.02	49.99	50.01
0.5	6	0.3	49.92	50.00	50.25

Table 4.2: CPW, design parameters for Z_0 = 50 Ω

The studied S-RRs and C-SRRs have the design parameters presented in Tables 3.5 and 3.6, respectively. However, for these values, the separation between the two S-SRR at 5 GHz is too small, and the two rings overlap, as shown in Figure 4.7. With this in mind, a new CPW is designed exclusively for this case, with parameters summarized in Table 4.3. As it can be seen, the characteristic impedance is around 75 Ω. Nevertheless, this structure was chosen as it prevents the overlap of the resonators.

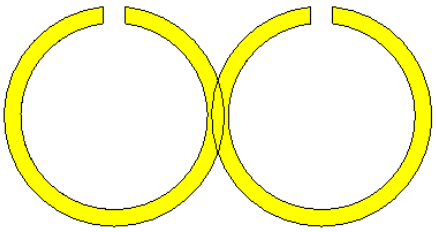

Figure 4.7: CPW, overlapped S-SRR

h (mm)	**w** (mm)	**g** (mm)	Z_0 (Ω) (f =5 GHz)
0.127	8	1	76.5
0.254	7	1	75.5
0.5	5.5	1.1	76.1

Table 4.3: CPW, new values for S-SRR

Influence of substrate height

The height of the substrate, as explained in Section 3.3, has a direct influence in the coupling of the resonators and the CPW. When its value increments, the coupling for the S-SRR decreases, whereas for the S-CSRR it improves until one critical value.

In Figure 4.3 a) and b) the frequency shift for the S-SRRs and S-CSRRs for the three aforementioned heights is displayed. From it, the relative shift in the S-SRRs is slightly better for the one with resonance at 15 GHz and a height of 0.5 mm, due to having a higher coupling for this configuration. Regarding the S-CSRR, the maximum frequency shift is achieved for a height of 0.127 mm and the resonator with resonance frequency of 5 GHz. For this structure, the coupling is higher than the other two, being this the reason of having a larger frequency shift. In conclusion, the resonators that are studied from on now are the S-SRR at 15 GHz and a substrate height of 0.5 mm and the S-CSRR with resonance at 5 GHz and substrate height of 0.127 mm.

It is also noteworthy that the shift for the S-CSRR is larger than for the S-SRR independently of the substrate height, as it happens for the microstrip line. The reason is, as aforestated in the previous section, that the sensing surface of the S-CSRR is larger than the one of the S-SRR.

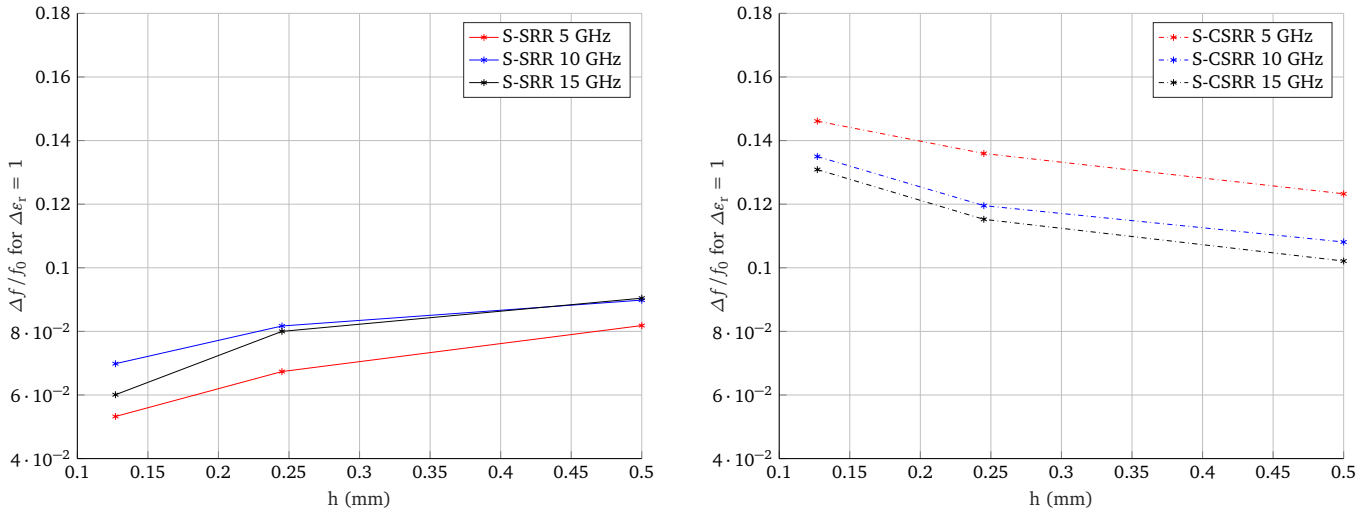

(a) S-SRR, $\Delta f/f_0$ vs substrate height

(b) S-CSRR, $\Delta f/f_0$ vs substrate height

Figure 4.8: CPW, $\Delta f/f_0$ in dependency of substrate height

Influence of θ of resonator regarding the strip

As it is explained before, the behaviour of the resonators is symmetric, so it is only necessary to study half of a total rotation of the resonator. From Section 3.3, it is concluded that the coupling is larger for the S-SRR in the CPW when the gap of the resonator is aligned with the central strip. Moreover, the S-CSRR presents a maximum coupling value when its gap is in the opposite side of the ring regarding the strip. In Figure 4.9 the simulation results of the relative Δf for both resonators are displayed.

For both of them, it can be seen that the highest frequency shift is achieved when $\theta = 0°$ or $180°$. In other words, when the gaps of the resonators are orthogonal regarding the electric field of the cpw, so its influence in the excitation is maximum. Moreover, the shift for the S-CSRR is almost constant. This is due the low coupling to the CPW. Consequently, both resonators are aligned in the direction of the central strip for the following simulations.

Influence of resonator width w

Similar to the investigation with the microstrip line, increasing the resonator width for the S-SRR means to increase both the losses of the structure and the electric field amplitude at the gap. Thus, the frequency shift depends on which one of the two effects predominates. For instance, when the losses are large enough, the relative frequency shift decreases. Moreover, for the S-CSRR the shift increases. This is due to the decrease of metallization, which reduces the losses of the structure. Furthermore, the coupling to the CPW is strong enough to achieve an almost constant electric field on the ring for the studied ring widths.

In Figure 4.10, the relative Δfs obtained from simulation results for different resonator widths are displayed. In consequence, the S-SRR is chosen to have a width of 0.35 mm, since the shift is not substantially different for each case. Furthermore, the width for the S-CSRR is selected to be 2.125 mm, as it presents the larger frequency shift.

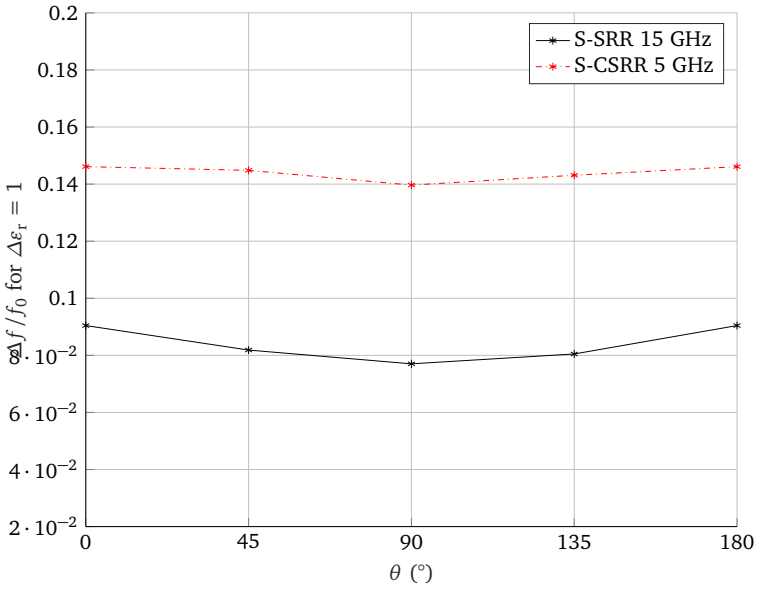

Figure 4.9: CPW, $\Delta f/f_0$ in dependency of θ

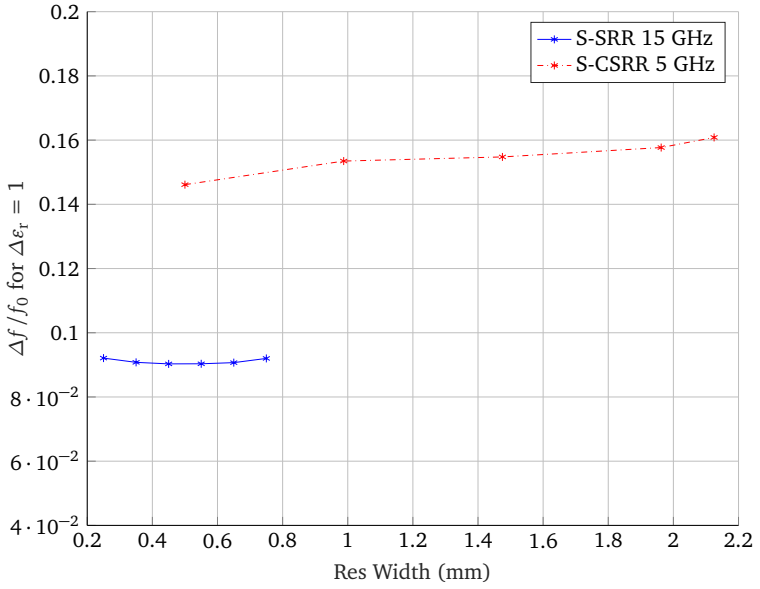

Figure 4.10: CPW, $\Delta f/f_0$ in dependency of width of resonator

Influence of gap width g

For large gap widths of the S-SRR, the electric field amplitude in its vicinities is lower due the separation between both metallic parts of the gap. However, for this case the differences between the possible values for the gap width are minuscule, since the overall size of the resonator is already small. Thus, the frequency shift has not a significant dependence on this parameter os the S-SRR. For the S-CSRR, a large metallic gap means that the concentration of the electric field in the ring is higher, for the same coupling, as the space that can be occupied by it decreases. Thus, the shift that it experiments is larger.

In Figure 4.11, the relative frequency shift for different width of the gap is displayed for both resonators. As it is stated, the shift for the S-SRR is not altered significantly, whereas for the S-CSRR is enhanced for larger widths of the gap. In consequence, the selected gap widths for the S-RR and S-CSRR are 0.5 mm and 2.675 mm, respectively, as they offer a relatively good shift and coupling to the coplanar waveguide. When

the gap width for the S-CSRR is further increased, the resulting structure is a hybrid of square and circular resonator.

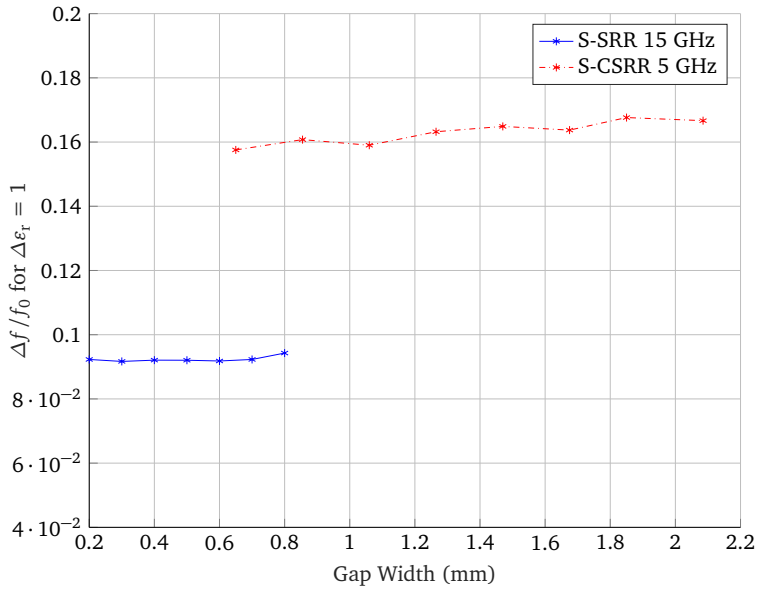

Figure 4.11: CPW, $\Delta f/f_0$ in dependency of width of gap

4.3 Sensitivity

In this Section, the figure of merit (FoM) explained in 4.1 is applied to the four structures that were optimized regarding the relative frequency shift in order to determine the best structure for sensitivity applications. For that, three dielectric blocks of $\varepsilon_r = 2$, 15 and 20 are used.

First of all, the four structures parameters are summarized and compared to the ones before being optimized in terms of resonance frequency. Then, the FoM is applied.

Since the substrate Rogers R04003C was out of stock, it has been changed to Rogers RO4350B, whose $\varepsilon_r = 3.48$, instead of the 3.38 of the former substrate. Moreover, the height of both S-CSRR has been changed to 0.17 mm. As the difference between the parameters is not large, the previous results can still be applied.

4.3.1 Optimized structures

During the optimization process, the design parameters of the resonators were modified, with the result of having a resonance frequency not exactly as the original resonances at 5 GHz, 10 GHz and 15 GHz. Consequently, Table 4.4 displays the design parameters and resonance frequency for the first resonators, compared with the optimized structures in terms of frequency shift. For this table, r is the radii of the resonators, h is the substrate height, w is the resonator width and g the resonator gap width.

From Table 4.4 it is noticeable that the resonance for S-SRR stays around 15 GHz. This is due to the overall limited size of the resonator, which only allows for small changes in its parameters. In opposition, for both S-CSRR the resonance presents a shift of more than 3 GHz. Concretely, 3.645 GHz when coupled to microstrip line and 3.22 GHz when coupled to CPW. The explanation of this large shift in the resonance can be understood in terms of the resonator width. As it is displayed in the Table, the rings of the optimized S-CSRRs are remarkably wider than the previous ones. In Section 2.2 it is explained that for large resonator widths, the resonance in S-CSRR is shifted to higher values, due to the decreasing of the total capacitance of the structure.

	Resonator	**r** (mm)	f_0 (GHz)	**h** (mm)	**w** (mm)	**g** (mm)
Microstrip	$S-SRR_{\text{old}}$	1.2	15	0.5	0.35	0.25
	$S-SRR_{\text{new}}$	1.2	15.16	0.5	0.45	0.15
	$S-CSRR_{\text{old}}$	3.6	5.01	0.5	0.5	0.65
	$S-CSRR_{\text{new}}$	3.6	8.745	0.17	1.85	1.85
CPW	$S-SRR_{\text{old}}$	1.3	15.35	0.5	0.5	0.65
	$S-SRR_{\text{new}}$	1.3	16.1	0.5	0.35	0.5
	$S-CSRR_{\text{old}}$	3.8	5.01	0.5	0.5	0.65
	$S-CSRR_{\text{new}}$	3.8	8.32	0.17	2.125	1.675

Table 4.4: Comparison between old and new resonators

4.3.2 Figure of merit

The FoM, as defined in Section 4.1, takes into account the relative resonance shift when the resonator is loaded with a material, as well as the normalized bandwidth B_{1dB}/f_0 as is defined in Equation 4.4. This bandwidth is selected due to having simulation results where the resonance peak on $|S_{21}|$ is located in higher values than 3 dB. This is a consequence of loading structures with relatively low coupling with dielectric blocks of large ε_r. By selecting that bandwidth, it is possible to obtain accurately the bandwidth of all the structures. Thus, the information has to be extracted from the $|S_{21}|$ of the different resonators, to be able to obtain the values to apply the FoM. In Table 4.5 and Table 4.6 the sensitivity observations are displayed for the four structures.

	$\Delta\varepsilon_r$	$f_{0,\text{loaded}}$	Δf (MHz)	$B_{\mathbf{1dB}}$ (MHz)	**FoM**	**FoM** (dB)
S-SRR	1	13.885	1275	231	5.52	7.42
	14	7.735	7425	267	27.81	14.42
	19	6.885	8275	623	13.28	11.26
S-CSRR	1	7.29	1455	251	5.8	7.63
	14	3.225	5520	33.9	162.83	22.11
	19	2.82	5925	46.7	126.87	21.03

Table 4.5: Sensitivity observations of microstrip structure

	$\Delta\varepsilon_r$	$f_{0,\text{loaded}}$ (GHz)	Δf (MHz)	$B_{\mathbf{1dB}}$ (MHz)	**FoM**	**FoM** (dB)
S-SRR	1	12.075	4025	346	11.63	10.66
	14	6.8	9300	235	39.57	15.97
	19	6.15	9950	167	59.58	17.75
S-CSRR	1	6.94	1380	611	2.26	3.54
	14	2.97	5350	227	23.57	13.72
	19	2.58	5740	128	44.84	16.52

Table 4.6: Sensitivity observations of CPW structure

On the one hand, from Table 4.5 it can be seen that the FoM for the S-CSRR presents better results than for the S-SRR. This is due to the stronger coupling of this structure to the transmission line, which allows for an easy recognition of the resonance. Although the frequency shift experimented by the S-SRR is larger, its coupling to the microstrip is extremely low compared to the S-CSRR, which causes a broad bandwidth in resonance. Thus, it is penalized by the FoM, specially for dielectric blocks with large ε_r. As an observation, this is an example of how the FoM is able to successfully discriminate between structures with large frequency shift but broad resonance bandwidth, and structures whose resonance frequency shift is shorter but present a narrower bandwidth at resonance.

On the other hand, the results in Table 4.6 displays that the best result for the CPW is obtained by the S-SRR. This is caused by the stronger coupling of this structure to the transmission line in comparison to the S-CSRR, which allows for a narrower resonance bandwidth.

In lights of the above, it is clear that the S-CSRR coupled to the microstrip line is the most suitable option of the four structures in terms of sensitivity. Although for $\varepsilon_r = 1$ its FoM is not the best, in the other two dielectric blocks, $\varepsilon_r = 15$ and 20, it shows the best performance by far. This means, it is able to successfully distinguish between materials with high dielectric permittivity. Moreover, it presents a large resonance frequency shift versus a narrow bandwidth, that allows for an easy recognition and detection of resonance. Thus, this structure is the chosen one to be fabricated.

5 Realization and measurement

From previous investigations, the S-CSRR coupled to microstrip line was found to have the best performance. Therefore, is was fabricated in order to prove the simulation results. The design parameters for the final structure are summarized in Tables 5.1 and 5.2.

h (mm)	**w** (mm)	**Length** (mm)	Z_0 (Ω) (f =5 GHz)
0.17	0.28	30	58.64

Table 5.1: Microstrip, final design parameters

From Table 5.1, it can be seen that the characteristic impedance of the transmission line is 58.64 Ω. This is caused by having changed the height of the substrate from the h=0.127 mm studied in Chapter 3, to the h=0.17 mm considered in Chapter 4, as the previous height was not available to use in the fabrication of the structure. For the last one, the strip width was not modified to preserve the coherence of the study made in Chapter 3. Nevertheless, the signal energy that flows into the structure is the 92 % of the signal generated by the spectral vector analyser, which is inside a permissible margin to be able to use this results.

r (mm)	θ (°)	**w** (mm)	**g** (mm)	**h** (mm)	f_0
3.6	Aligned with strip	1.85	1.85	0.017	8.745

Table 5.2: S-CSRR, final design parameters

In Figure 5.1, both sides of the fabricated structure are displayed, in comparison to a 10 cents coin.

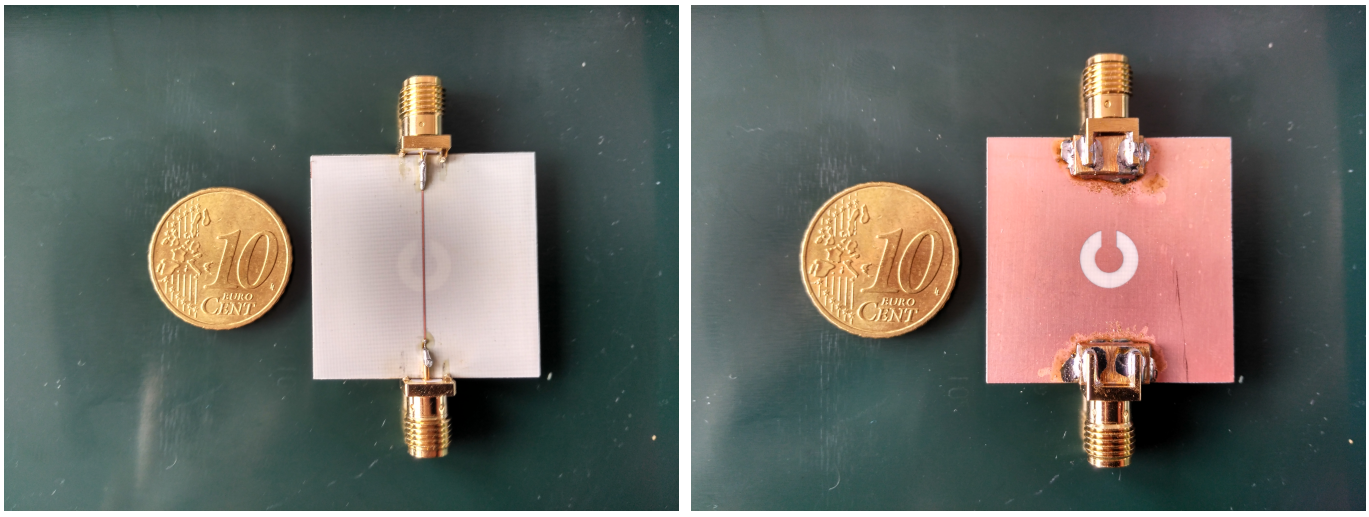

(a) Microstrip, top

(b) Microstrip, bottom

Figure 5.1: Fabricated structure

5.1 Measurement Set-up

The measurements are performed with the Spectral Vector Analyzer E5071C, from Agilent Technologies. It can measure frequencies responses from 300 kHz to 20 GHz. Thus, the fabricated structure is inside its frequency range. The measurement is configured for a 2-Port network. The frequency range of the Analyzer is set from 1 GHz to 12 GHz, with 2001 steps. In consequence, the spectral resolution is 6 MHz.

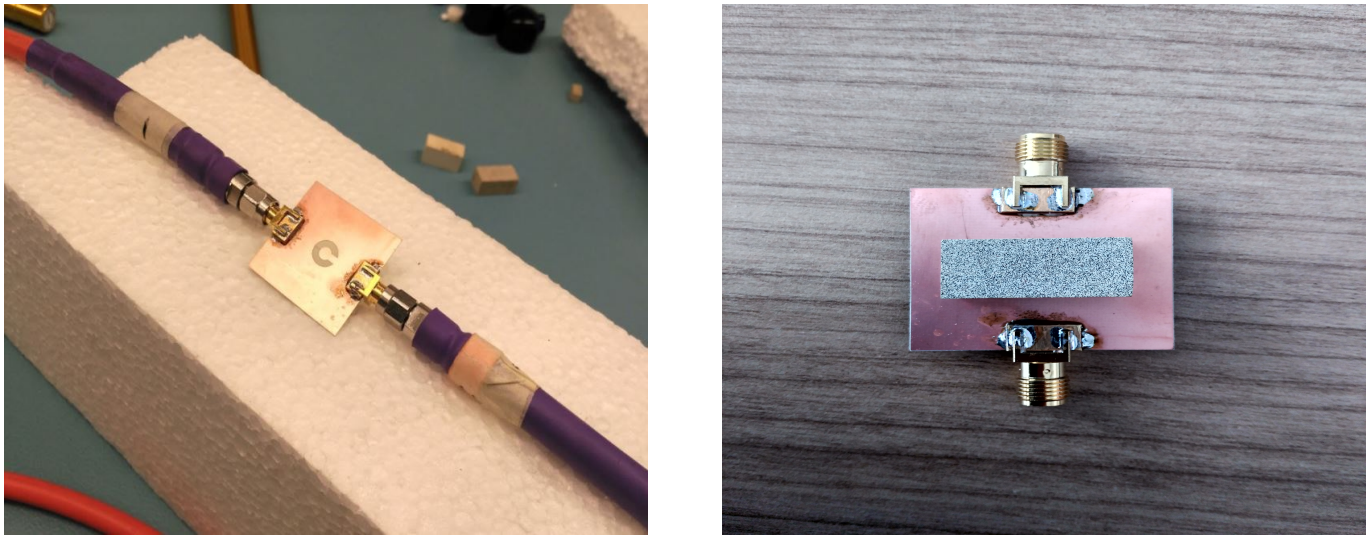

(a) Connection coaxial cables

(b) Example without cables

Figure 5.2: Measurement set up.

In order to carry out the measurements, two coaxial cables are connected to the fabricated device, as it is displayed in Figure 5.2 a). After that, different measurements of the S-parameters of the structure are performed. The resonator is loaded with materials of different permittivity, as shown in 5.2 b). Four evaluations are made. First of all, when the resonator is unloaded. After that, it was loaded with dielectric bricks of $\varepsilon_r = 2$, which is Teflon, $\varepsilon_r = 15$ or Brick 1, and finally $\varepsilon_r = 20$, also written as Brick 2.

During this process, it was necessary to pay an important amount of attention to the structure, since it is very flexible due to its thinness. Thus, it is very easy to unconsciously bend it. This is reflected on the S-parameters of the structure, with the introduction of unintended reflections in the structure.

5.2 Results

In Figure 5.3, the $|S_{21}|$ parameters are measured for each different dielectric and compared with the simulations. It is specially important the result obtained for both unloaded resonators, a), since it indicates that the simulated model and the fabrication are very accurate, as the resonance frequency is almost the same. Moreover, the coupling for the real case is higher than the simulations. The slightly differences outside the resonance are caused by the involuntary bending of the substrate, which produces reflections. It can also be seen that for resonators that are loaded there is a variation in the resonances of around 1 GHz regarding the simulated results and measurements. This is caused by the losses of the dielectric blocks, which were not considered during the simulations. This shift might also be enhanced by the presence of small air gaps between the resonator and the dielectric blocks, due to the bending of the structure, as the measurements were done by manually placing the blocks in the structure.

In order to be able to apply the FoM to the measurements, it is necessary to calculate the frequency shift regarding the unloaded resonance and the bandwidth for each loaded structure. In Figure 5.4 a) a comparison

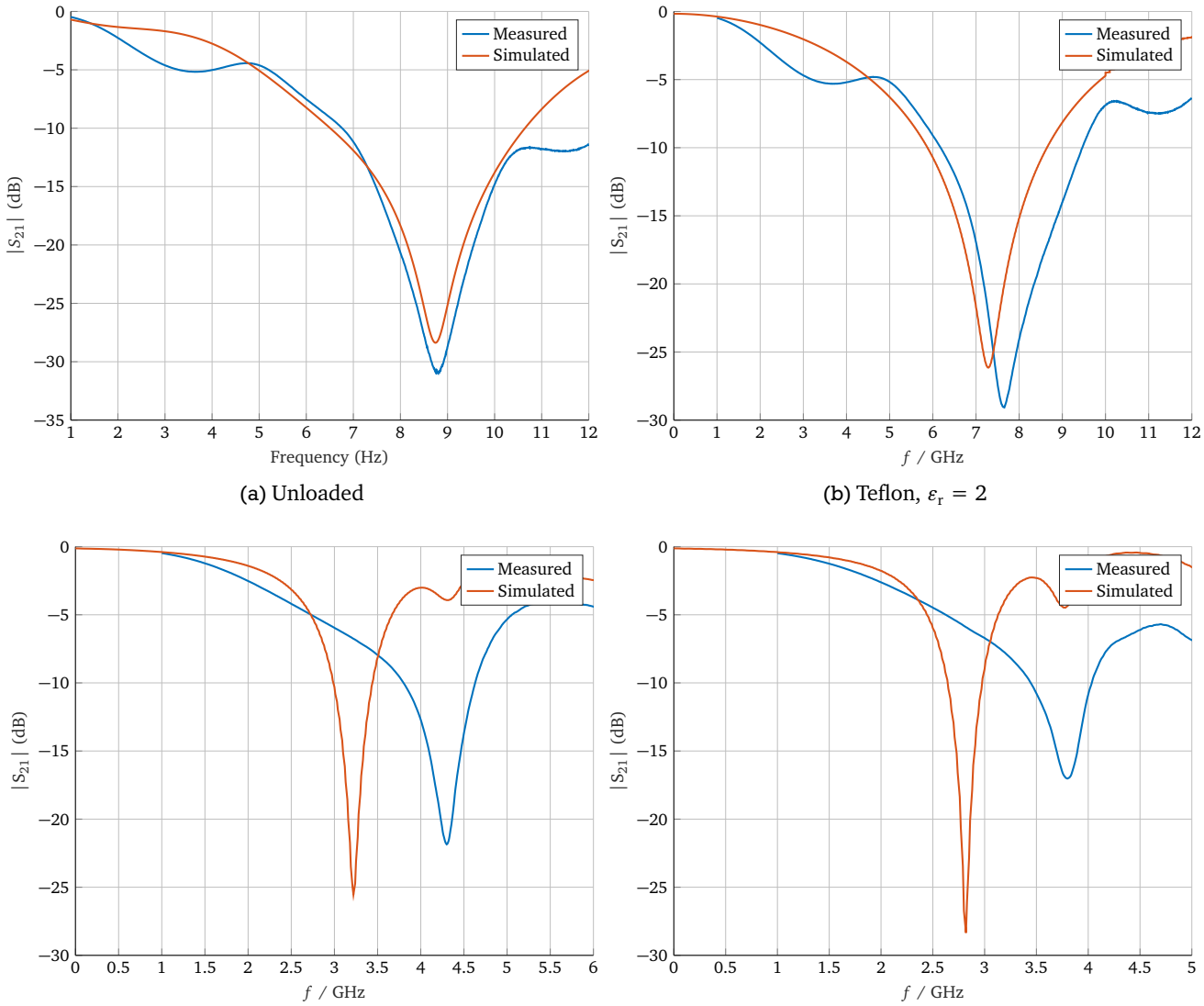

(a) Unloaded

(b) Teflon, $\varepsilon_r = 2$

(c) Brick 1, $\varepsilon_r = 15$

(d) Brick 2, $\varepsilon_r = 20$

Figure 5.3: Comparison of $|S_{21}|$ between simulation and measurements

between the resonance of the unloaded fabricated structure and when it is loaded with Teflon can be seen. In Figure 5.4 b), the same comparison is showed for the two dielectric bricks of $\varepsilon_r = 15$ and 20. From these graphs, the necessary Δf and $B_{1\text{dB}}$ can be obtained. In this Figure, it is also easily noticeable the resonance shift produced when loading the structure, as well as narrow bandwidth. Thus, the resonance can be easily detected.

The results when applying the FoM to measurements are displayed in Table 5.3. They are also compared to the values from simulation. In light of the results, it can be seen that the shift for measurements is shorter than for the simulations and their bandwidths are broader. This is caused by the lossy dielectric blocks, that were considered to be lossless during the simulations. Consequently, when using the FoM for these measurements, it is expected that it worsens. From Table 5.3, this statement is confirmed. The differences between responses for simulations and measurements is due, as aforementioned, to the lossy dielectric blocks used in the measurements. This effect might be enhanced due to the presence of small air gaps between the dielectric and the resonator, which decreases the effective permittivity of the system and thus the frequency shift.

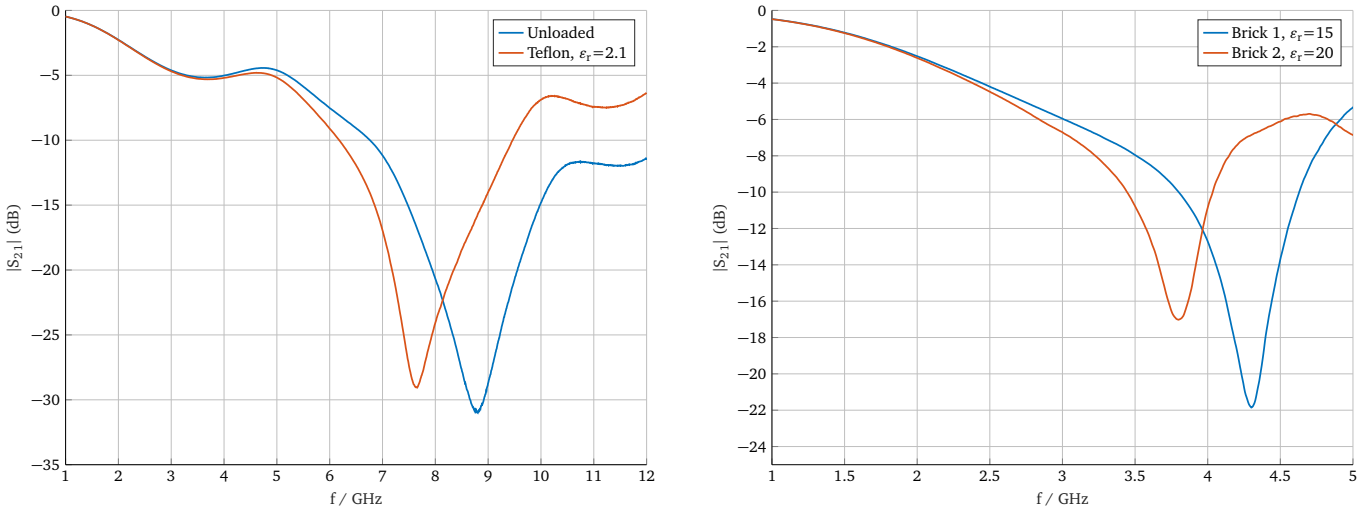

(a) Unloaded vs Teflon

(b) Brick 1 vs Brick 2

Figure 5.4: Comparison of $|S_{21}|$ between measurements

	$\Delta\varepsilon_r$	$f_{0,\text{loaded}}$ (GHz)	Δf (MHz)	$B_{\text{-1dB}}$ (MHz)	**FoM**	**FoM** (dB)
S-CSRR$_{\text{Simul.}}$	1	7.29	1455	251	5.8	7.63
	14	3.225	5520	33.9	162.83	22.11
	19	2.82	5925	46.7	126.87	21.03
S-CSRR$_{\text{Measurm.}}$	1	7.529	1156	214	5.4	7.33
	14	4.245	4500	94	47.87	16.8
	19	3.745	5000	140	35.7	15.53

Table 5.3: Comparison of sensitivity between measurements and simulations

6 Conclusion & Outlook

The aim of this bachelor thesis was to describe S-SRR and S-CSRR in terms of their coupling to planar transmission lines and performance in terms of sensitivity. Therefore, full wave simulations were done using CST Studio, by exciting the S-SRR and the S-CSRR with a axial magnetic or electric field regarding their ring, respectively. It was described how their design parameters affect their resonance frequency, being the radius the parameter that is the most influential.

After this, the coupling to planar TL was studied. It was found that S-CSRR provide better coupling with microstrip lines. This is because they are located on the ground of the microstrip, which allows them to be directly excited with the inherent electric field of the TL, that is axial to its ring. In contrast, the S-SRR presents a larger coupling for the CPW, due to its magnetic field being radial to the ring of the resonator.

Generally, the coupling of both resonators is mainly influenced by the substrate height and the angle of the resonator. By decreasing the first, the coupling to TL can be increased. Regarding the angle, it can increase the excitation of the resonators by being placed in the same direction of the strip of the TL.

A sensitivity analysis was done for the resonators coupled to a microstrip line and a CPW, by defining a figure of merit that takes into account large frequency shifts and sharp resonance peaks. It was seen that for the three different substrate heights, S-CSRRs provided better sensitivity for thin substrates, whereas the performace of S-SRRs was higher with the thickest substrate. Moreover, the position of the gap of the resonators plays a significant role to enhance the sensitivity by locating it aligned to the strip of the TL. Finally, four structures were selected and compared. As a result, the S-CSRR coupled to microstrip line was found to have the best sensitivity, due to its strong coupling and larger sensing surface.

In order to measure the performance of the selected structure, it was fabricated on the substrate Rogers RO4350B with a height of 0.17 mm. It was found that for the structure surrounded by air the measurements fitted well to the simulations. When loading the structure with different dielectric bricks, $\varepsilon_r = 2.1$,15 ,20; there was a divergence in the resonance with shifts of 1 GHz between the simulated and measured results for materials with high permittivity. A possible reason is that the bricks were put manually on the ring structure with a probable presence of small air gaps between them and the resonator.

In conclusion, S-SRRs present lower performance that their Complementary structures, due to their smaller sensing surface. Thus, in the area of biological detection, S-CSRR resonators can be considered as a better option to determine dielectric properties of tissue, when coupled to planar TL compared to S-SRR.

For future work, the integration of the S-CSRR coupled to microstrip lines into a needle-like surgery tool must be adressed. This can be achieved by rolling the relatively thin and flexible substrate to form a cylindrical shape, as explained in [28]. Moreover, the ablation properties of the S-CSRRs at different frequencies like 5, 10 and 15 GHz have to be evaluated to find a good compromise for a theranostic microwave applicator.

Bibliography

[1] "The burden." [Online]. Available: http://canceratlas.cancer.org/the-burden/

[2] "Cancer." [Online]. Available: http://www.who.int/mediacentre/factsheets/fs297/en/

[3] "Global action plan for the prevention and control of ncds 2013-2020." [Online]. Available: http://www.who.int/nmh/events/ncd_action_plan/en/

[4] "Types of cancer treatment." [Online]. Available: https://www.cancer.gov/about-cancer/treatment/types

[5] "Side effects." [Online]. Available: https://www.cancer.gov/about-cancer/treatment/side-effects

[6] M. Puentes, F. Bashir, M. Schussler, and R. Jakoby, "Dual mode microwave tool for dielectric analysis and thermal ablation treatment of organic tissue," *2012 Annual International Conference of the IEEE Engineering in Medicine and Biology Society*, 2012.

[7] M. Puentes, M. Maasch, M. Schubler, and R. Jakoby, "Frequency multiplexed 2-dimensional sensor array based on split-ring resonators for organic tissue analysis," *IEEE Transactions on Microwave Theory and Techniques*, vol. 60, no. 6, pp. 1720–1727, 2012.

[8] C. M. S. Jiangfeng Zhou, Thomas Koschny, "Magnetic and electric excitations in split ring resonators," *Optics Express*, vol. 15, no. 26, dec 2007.

[9] D. M. Pozar, *Microwave engineering*. Wiley, 2012.

[10] W. Hardy and L. Whitehead, "Split-ring resonator for use in magnetic resonance from 200-2000 mhz," *AIP Rev. Sci. Instrum*, vol. 52, no. 2, pp. 213–216, 1981.

[11] J. S. Hyde and W. Froncisz, "Loop gap resonators," *Advanced EPR*, pp. 277–305, 1989.

[12] M. Mehdizadeh, T. Ishii, J. Hyde, and W. Froncisz, "Lumped mode microwave resonant structures," *MTT-S International Microwave Symposium Digest*, pp. 1059–1068, Dec 1983.

[13] O. Sydoruk, E. Tatartschuk, E. Shamonina, and L. Solymar, "Analytical formulation for the resonant frequency of split rings," *Journal of Applied Physics*, vol. 105, no. 1, p. 014903, jan 2009. [Online]. Available: https://doi.org/10.1063/1.3056052

[14] N. Katsarakis, T. Koschny, M. Kafesaki, E. N. Economou, and C. M. Soukoulis, "Electric coupling to the magnetic resonance of split ring resonators," *Applied Physics Letters*, vol. 84, no. 15, pp. 2943–2945, apr 2004. [Online]. Available: https://doi.org/10.1063/1.1695439

[15] K. Aydin, I. Bulu, K. Guven, M. Kafesaki, C. M. Soukoulis, and E. Ozbay, "Investigation of magnetic resonances for different split-ring resonator parameters and designs," *New Journal of Physics*, vol. 7, pp. 168–168, Aug 2005.

[16] M. Born and E. Wolf, *Principles of Optics*. Cambridge University Press, Cambridge, 1999.

[17] C. L. Andrews and D. P. Margolis, "Elemental derivation of the babinet principle in electromagnetic form," *American Journal of Physics*, vol. 43, no. 8, pp. 672–676, 1975.

[18] Z. M. Tan and K. T. McDonald, "Babinet's principle for electromagnetic fields," *Joseph Henry Laboratories, Princeton University, Princeton, NJ 08544*, 2012, updated on December 20, 2016.

[19] M. Y. Dimyan, “Propagation characteristics of microstrip transmission lines on intrinsic germanitnn substrates,” Master’s thesis, McMASTER UNIVERSITY, Hamilton, Ontario, 1969.

[20] T. D. Bahl, I.J., “A designer’s guide to microstrip line,” *Microwaves*, vol. 16, no. 5, pp. 174–182, 1977.

[21] R. Garg, *Microstrip antenna design handbook*. Artech House, 2001.

[22] “Microstrip ads and linecalc.” [Online]. Available: http://examcrazy.com/Engineering/Electronics-Communication/Microstrip_ADS_and_LineCalc.asp

[23] C. Wen, “Coplanar waveguide, a surface strip transmission line suitable for nonreciprocal gyromagnetic device applications,” *1969 G-MTT International Microwave Symposium*, 1969.

[24] S. Gevorgian, T. Martinsson, A. Deleniv, E. Kollberg, and I. Vendik, “Simple and accurate dispersion expression for the effective dielectric constant of coplanar waveguides,” *IEE Proceedings - Microwaves, Antennas and Propagation*, vol. 144, no. 2, p. 145, 1997.

[25] “Coplanar waveguides (cpw).” [Online]. Available: http://qucs.sourceforge.net/tech/node86.html

[26] S. Pinon, D. L. Diedhiou, A.-M. Gue, N. Fabre, G. Prigent, V. Conedera, E. Rius, C. Quendo, B. Potelon, J.-F. Favennec, and et al., “Development of a microsystem based on a microfluidic network to tune and reconfigure rf circuits,” *Journal of Micromechanics and Microengineering*, vol. 22, no. 7, p. 074005, 2012.

[27] A. P. O’Rourke, M. Lazebnik, J. M. Bertram, M. C. Converse, S. C. Hagness, J. G. Webster, and D. M. Mahvi, “Dielectric properties of human normal, malignant and cirrhotic liver tissue:in vivoandex vivomeasurements from 0.5 to 20 ghz using a precision open-ended coaxial probe,” *Physics in Medicine and Biology*, vol. 52, no. 15, p. 4707-4719, 2007.

[28] C. Reimann, M. Puentes, H. Maune, R. Jakoby, B. Bazrafshan, F. Hubner, and T. J. Vogl, “A cylindrical shaped theranostic applicator for percutaneous microwave ablation,” *IMBioC Gothenburg, Sweden*, May 2017.

List of Figures

List of Tables